Article

Cell Reports

Dectin-1 Binding to Annexins on Apoptotic Cells Induces Peripheral Immune Tolerance via NADPH Oxidase-2

Graphical Abstract

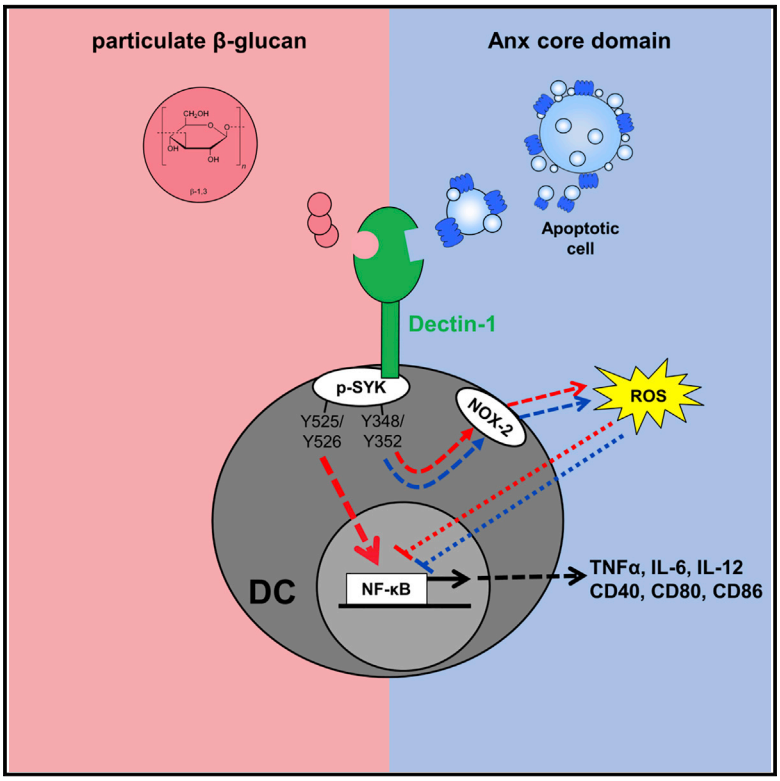

Authors

Kevin Bode, Fatmire Bujupi, Corinna Link, ..., Bernd Lepenies, Heiko Weyd, Peter H. Krammer

Correspondence

p.krammer@dkfz-heidelberg.de (P.H.K.), h.weyd@dkfz-heidelberg.de (H.W.)

In Brief

Bode et al. identify Dectin-1 on dendritic cells as a receptor for apoptotic-cell-bound annexins responsible for the induction of peripheral immune tolerance. Tolerogenic signaling depends on selective SYK phosphorylation and the production of reactive oxygen species via NADPH oxidase-2. Dectin-1-deficient mice generate stronger immune responses against apoptotic cells and develop autoimmunity.

Highlights

- Dectin-1 is a tolerogenic receptor for annexins on the surface of ACs
- Annexin-binding to Dectin-1 induces selective SYK phosphorylation
- SYK-dependent ROS production via NOX-2 is critical for tolerogenic signaling
- Dectin-1 deficiency causes autoimmunity

Bode et al., 2019, Cell Reports *29*, 4435–4446
December 24, 2019
https://doi.org/10.1016/j.celrep.2019.11.086

CellPress

Cell Reports
Article

Dectin-1 Binding to Annexins on Apoptotic Cells Induces Peripheral Immune Tolerance via NADPH Oxidase-2

Kevin Bode,[1,2] Fatmire Bujupi,[1,2] Corinna Link,[1,2] Tobias Hein,[1,2] Stephanie Zimmermann,[3,4] Diluka Peiris,[5] Vincent Jaquet,[6] Bernd Lepenies,[3,7] Heiko Weyd,[1,8,*] and Peter H. Krammer[1,8,9,*]

[1]Division of Immunogenetics, Research Program Immunology and Cancer, German Cancer Research Center, 69120 Heidelberg, Germany
[2]Faculty of Biosciences, Ruprecht Karls University Heidelberg, 69120 Heidelberg, Germany
[3]Department of Biomolecular Systems, Max Planck Institute of Colloids and Interfaces, 14476 Potsdam, Germany
[4]Department of Biology, Chemistry and Pharmacy, Free University Berlin, 14195 Berlin, Germany
[5]Attana AB, Greta Arwidssons v. 21, 11419 Stockholm, Sweden
[6]Department of Pathology and Immunology, University of Geneva, 1211 Geneva, Switzerland
[7]Immunology Unit and Research Center for Emerging Infections and Zoonoses, University of Veterinary Medicine Hannover, 30559 Hannover, Germany
[8]These authors contributed equally
[9]Lead Contact
*Correspondence: p.krammer@dkfz-heidelberg.de (P.H.K.), h.weyd@dkfz-heidelberg.de (H.W.)
https://doi.org/10.1016/j.celrep.2019.11.086

SUMMARY

Uptake of apoptotic cells (ACs) by dendritic cells (DCs) and induction of a tolerogenic DC phenotype is an important mechanism for establishing peripheral tolerance to self-antigens. The receptors involved and underlying signaling pathways are not fully understood. Here, we identify Dectin-1 as a crucial tolerogenic receptor binding with nanomolar affinity to the core domain of several annexins (annexin A1, A5, and A13) exposed on ACs. Annexins bind to Dectin-1 on a site distinct from the interaction site of pathogen-derived β-glucans. Subsequent tolerogenic signaling induces selective phosphorylation of spleen tyrosine kinase (SYK), causing activation of NADPH oxidase-2 and moderate production of reactive oxygen species. Thus, mice deficient for Dectin-1 develop autoimmune pathologies (autoantibodies and splenomegaly) and generate stronger immune responses (cytotoxic T cells) against ACs. Our data describe an important immunological checkpoint system and provide a link between immunosuppressive signals of ACs and maintenance of peripheral immune tolerance.

INTRODUCTION

Removal of apoptotic cells (ACs) is closely associated with the induction of immunological self-tolerance. Each day, billions of ACs are phagocytosed by antigen-presenting cells such as dendritic cells (DCs) and actively modulate the immune response (Vaux and Korsmeyer, 1999). Following engulfment of ACs, DCs acquire a tolerogenic phenotype characterized by low expression of co-stimulatory surface molecules and inflammatory cytokines as well as resistance to activation (Morelli and Thomson, 2007). These tolerogenic DCs process AC-derived self-antigens and present them to naive T cells, thereby inducing T cell tolerance (Voll et al., 1997; Tanaka et al., 2008; Mueller, 2010). While phagocytic receptors and their ligands on ACs are well described (Arandjelovic and Ravichandran, 2015), less is known about the tolerogenic signaling machinery engaged by ACs. Recently, we demonstrated that early ACs expose members of the annexin protein family on their surface (Weyd et al., 2013) that bind to negatively charged phospholipids such as phosphatidylserine (PS) in a Ca^{2+}-dependent manner (Gerke and Moss, 2002). It is well established that annexin A1 serves as an inhibitory signal to DCs and facilitates the development of peripheral tolerance (Yang et al., 1999; Pupjalis et al. 2011; Blume et al. 2009; Perretti and Dalli, 2009; Weyd et al., 2013; Linke et al., 2015). Structurally, all annexin family members contain an evolutionary conserved core domain and a unique N terminus. Immune regulatory functions such as neutrophil extravasation have mainly been described for annexin A1 and have been attributed to N-terminal binding to the N-formyl peptide receptor (FPR) family (Walther et al., 2000; Perretti et al., 2001). However, we found that the tolerogenic function mediated by the conserved annexin core domain is independent of FPRs (Linke et al., 2015). Specific receptors binding to the annexin core domain and mediating its tolerogenic effects remained elusive.

Dectin-1 (also known as Clec7a) belongs to the C-type lectin receptor (CLR) superfamily expressed on DCs, macrophages, and other immune cells. It serves as a pattern-recognition receptor with high affinity to β-1,3-linked glucans (β-glucans) (e.g., zymosan) present in cell walls of fungal and bacterial species. Thus, Dectin-1 is involved in the activation of immune responses following microbial and fungal infections (Plato et al., 2013; Dambuza and Brown, 2015; Brown et al., 2018). The induction of Dectin-1 signaling mainly depends on the tyrosine-based hemi-immunoreceptor activation motif in its cytoplasmic region, activating pathways through spleen tyrosine kinase (SYK), Raf-1, and Card-9. In addition, Dectin-1 stimulation by β-glucans leads to the downstream activation of nuclear factor kappa-light-chain-enhancer of activated

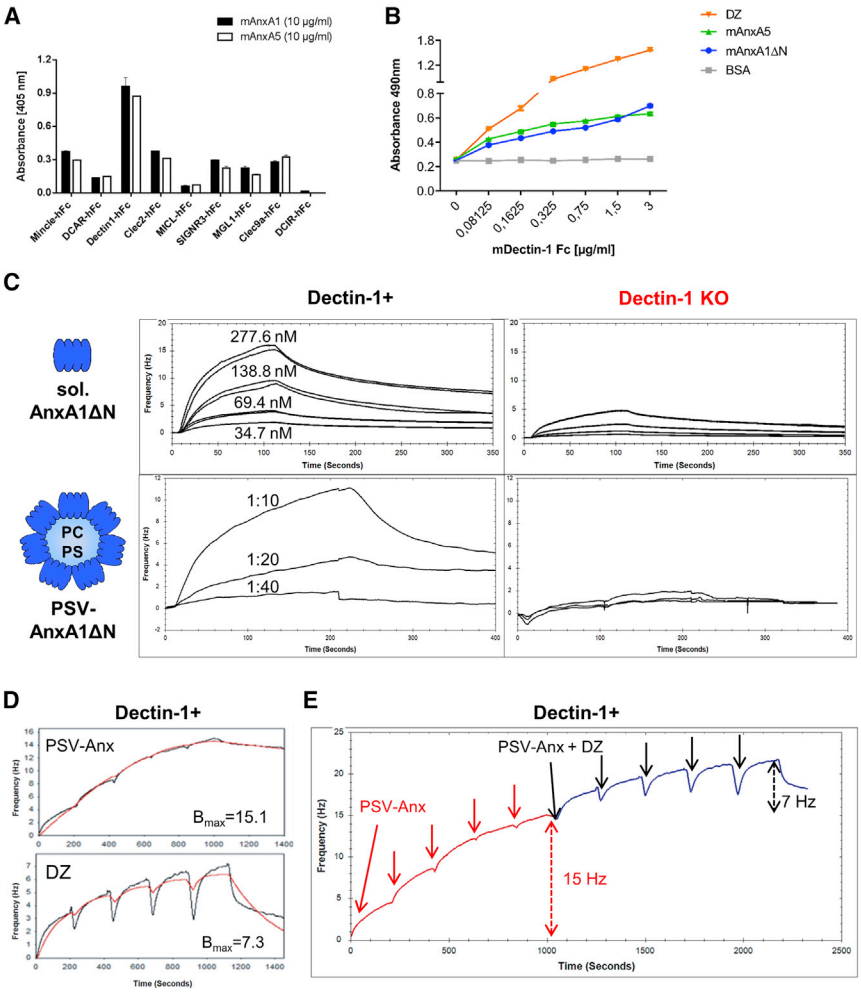

Figure 1. The Conserved Annexin Core Domain Is Recognized by Dectin-1 at Sites Distinct from β-Glucan-Binding Sites

(A and B) Murine annexin A1 (mAnxA1) (A), the core domain of annexin A1 (mAnxA1ΔN) (B), mAnxA5 (A and B), and depleted zymosan (DZ) or BSA (B) were immobilized and incubated with the indicated self-produced C-type lectin receptor (CLR) fusion proteins (A) or a commercially available mDectin-1 Fc (B).

(C) Interaction of purified human annexin A1ΔN (hAnxA1ΔN) (upper left and upper right panel) and annexin-A1ΔN-coated phosphatidylserine (PS) vesicles (PSV-Anx; lower left and lower right panel) with human Dectin-1 (hDectin-1)-expressing and Dectin-1 KO Mono Mac 6 (MM6) cells analyzed by quartz crystal microbalance technology. Both cell types were immobilized on Attana sensor surfaces. The signal output given in frequency (Hz) is directly related to changes in mass on the sensor surface (see STAR Methods).

(D) Characteristic binding responses of filtrated DZ (≤400 nm) and PSV-Anx to hDectin-1-expressing MM6 cells. The maximum binding capacity (B_{max}) value indicates the ligand specific frequency of fully saturated cell-surface binding (DZ ~7 Hz, PSV-Anx ~15 Hz).

(E) First, PSV-Anx was applied to the immobilized cells several times (red arrows; increasing amounts from left to right: 1:30, 1:25, 1:20, 1:15, and 1:10) until full binding response of PSV-Anx (~15 Hz) to the cell surface was obtained (also see STAR Methods). Next, a mixture of DZ and PSV-Anx was applied several times in same ratios (black arrows; increasing amounts from left to right: 1:30, 1:25, 1:20, 1:15, and 1:10) to investigate the occurrence of additional binding. PC, phosphatidylcholine. Results are representative of two independent experiments.

See also Figures S1 and S3 and Table S1.

B cells (NF-κB), among other signaling pathways (Schäppi et al., 2008; Reid et al., 2009; Dambuza and Brown, 2015).

In this study, we describe an immunosuppressive signaling pathway of ACs mediated by externalized annexins binding to Dectin-1. This receptor-ligand interaction constitutes an essential mechanism of peripheral immune tolerance by inducing a tolerogenic DC-phenotype in response to ACs.

RESULTS

The C-type Lectin Receptor Dectin-1 Binds to the Conserved Annexin Core Domain

We previously demonstrated that several annexin family members (annexin A1, A5, and A13) inhibit DC activation and induce antigen-specific $CD8^+$ T cell tolerance *in vivo* when exposed on the surface of ACs (Weyd et al., 2013; Linke et al., 2015). This immunosuppressive activity of annexins was confined to the conserved annexin core domain and was not mediated by members of the FPR family, which bind to the unique annexin A1 N terminus (Walther et al., 2000; Perretti et al., 2001; Linke et al., 2015). In search for a specific receptor binding to several annexin family members, we performed *in vitro* binding experiments using CLR-fragment crystallizable (Fc) library and recombinant annexins A1 and A5. Of all CLRs tested, we observed strong binding of both annexins to Dectin-1 only (Figure 1A). Since all annexin family members share the annexin core domain, these data suggest that Dectin-1 binds to the conserved core domain of various annexin family members. We confirmed the specific binding of Dectin-1 to the annexin A1 core domain by using a truncated version of annexin A1 (annexin A1ΔN) that lacks the N terminus (Figures 1B and S1A). Moreover, Fc-receptor-based surface plasmon resonance (SPR) experiments showed high-affinity binding of Dectin-1 to all annexins tested (annexin A1, annexin A1ΔN, annexin A5, and annexin A13; Figures S1B–S1F). We also confirmed the binding of Dectin-1 to annexins exposed on the surface of ACs (Figure S1G; Weck et al., 2008).

In order to investigate the Dectin-1/annexin interaction in a physiological context, we performed cell-based affinity measurements using quartz crystal microbalance (QCM) technology (see STAR Methods; Peiris et al., 2017; Salanti et al., 2015). We used stably transfected Dectin-1-expressing Mono Mac 6 (MM6) cells as well as CRISPR-Cas9-mediated Dectin-1 knockout (KO) MM6 cells (Figures S2A–S2C; Ziegler-Heitbrock et al., 1988; Ran et al., 2013) and soluble recombinant annexin A1ΔN and annexin

A5 as ligands. A Dectin-1-specific antibody and the Dectin-1 ligand depleted zymosan (DZ) served as positive controls. As expected, we observed increased binding of annexins to Dectin-1-expressing MM6 cells compared to the Dectin-1 KO MM6 cells (Figure 1 C; Table S1). However, we also detected high background binding to Dectin-1 KO cells, possibly due to interactions with negatively charged phospholipids such as PS exposed at low levels on the cell surface of living phagocytes (Callahan et al., 2000, 2003). To prevent background binding of annexins to PS, we generated defined PS-containing lipid vesicles and loaded them with annexin A1ΔN (Figure S2D). This way, the receptor-binding interface of annexin, as present on ACs, was still available for receptor interaction, while the PS-binding sites were occupied. Using annexin-coated lipid vesicles, we could demonstrate exclusive binding to Dectin-1-expressing MM6 cells (Figure S3B). Based on these results we conclude that Dectin-1 is a specific receptor for the PS-bound core domain of annexin A1 and other annexin family members.

To extend these data, we performed competitive QCM experiments to investigate whether annexins share the same binding site with classical pathogen-derived Dectin-1 ligands such as DZ. These experiments confirmed the exclusive binding of vesicle-bound annexin A1ΔN to Dectin-1-expressing MM6 cells (Figure 1C). We first determined the specific change of frequency for saturation of both ligands (15.1 Hz for annexin A1ΔN and 7.3 Hz for DZ on Dectin-1-expressing MM6 cells; Figures 1D and S3A). For competition experiments, we saturated Dectin-1-expressing MM6 cells with DZ and measured any additional changes in frequency upon subsequent injections of vesicle-bound annexin A1ΔN. Data shown in Figure 1E demonstrate that vesicle-bound annexin A1ΔN was still able to bind to DZ-saturated MM6 cells with kinetics identical to vesicle-bound annexin A1ΔN alone (Figures 1D and 1E). Moreover, we obtained similar results by applying the ligands in reverse order (Figure S3C). In summary, our data prove that the lipid-bound annexin A1 core domain binds to a distinct binding site of Dectin-1 not interfering with the binding of pathogen-derived β-glucans.

The Annexin Core Domain Induces Dectin-1-Dependent SYK-Phosphorylation and Production of Reactive Oxygen Species (ROSs)

One of the earliest signaling events downstream of β-glucan-mediated Dectin-1 activation is the phosphorylation of SYK by Src family kinases (Reid et al., 2009; Dambuza and Brown, 2015). To test whether the annexin core domain initiates Dectin-1-dependent SYK-phosphorylation, we used an antibody recognizing intracellular SYK-phosphorylation on Tyr348. In MM6 and primary bone-marrow-derived DCs (BMDCs), soluble annexin A1ΔN induced Tyr348 SYK-phosphorylation in a Dectin-1-dependent manner (Figures 2A, 2B, and S4C). In line with the effects of soluble annexin A1ΔN, this phosphorylation of SYK was also observed upon incubation with vesicle-bound annexin A1ΔN and ACs (Figures S4A and S4B). Interestingly and in correlation with the unique Dectin-1 binding modality described above, the kinetics of SYK-phosphorylation proved to be different between annexin A1ΔN and β-glucans. While DZ induced a long-lasting SYK-phosphorylation (≥30 min), annexin-mediated SYK-phosphorylation was characterized by a short peak after 15 min, which declined quickly to baseline level (Figure 2C; data not shown). To investigate the differences between Dectin-1-mediated β-glucan and annexin signaling, respectively, we analyzed the phosphorylation status of SYK in more detail. Our results clearly show that the annexin core domain as well as soluble, filtered β-glucan (0.45 μm membrane) induces phosphorylation of Tyr348 and Tyr352 within the SH2/SH3-linker of SYK, which allows for association and activation of phospholipase C (PLC) isotype γ (PLCγ) and leads to induction of ROSs (Law et al., 1996; Figure 2D). Interestingly, phosphorylation on Tyr525/526 of the SYK activation loop, required for NF-κB activation, remained unphosphorylated upon annexin incubation (Figure 2D). In contrast, large particulate β-glucans induced strong phosphorylation of all tyrosines investigated (Tyr348, Tyr352, and Tyr525/526; Figure 2D).

Dectin-1 engagement and SYK-phosphorylation on Tyr348 and Tyr352 lead to subsequent generation of ROSs (Blanco-Menéndez et al., 2015; Reid et al., 2009; Law et al., 1996). Measuring cellular ROS levels after stimulation with annexin A1ΔN using 2′,7′-dichlorodihydrofluorescein diacetate (H_2DCFDA), we detected a time-dependent increase of ROS production peaking after 2 h (Figure S4D). We confirmed the annexin A1ΔN-mediated ROS-induction using the horseradish-peroxidase-based Amplex Red Assay Kit (Figure S4E). Using BMDCs and MM6 cells, we were able to demonstrate that annexin-mediated generation of ROSs clearly is a Dectin-1-dependent effect observed after treatment with soluble and vesicle-bound annexin A1ΔN or annexin A5, respectively (Figures 2E–2G). The specificity of these assays was further assessed by using heat-inactivated annexin as well as the specific ROS scavenger Trolox (Figure 2E). Consistently, reconstitution of Dectin-1 expression in Dectin-1 KO MM6 cells could rescue the annexin-mediated phenotype with respect to ROS production (Figure S4F). Of note, Dectin-1-independent ROS induction by phorbol 12-myristate 13-acetate (PMA) was unaltered in all cellular systems. Furthermore, inhibition of SYK-phosphorylation abrogated the annexin A1ΔN-mediated ROS increase, indicating that annexin A1ΔN induces a SYK-dependent ROS signal (Figure 2H). Taken together, these data show that the annexin A1 core domain and annexin A5 serve as endogenous ligands for the CLR Dectin-1, leading to selective SYK-phosphorylation on Tyr348 and Tyr352 and ROS production. In comparison to the oxidative burst provoked by PMA or pathogen-derived DZ in BMDCs, annexin treatment induces moderate ROS levels, indicative of its role in signaling cascades rather than in β-glucan-mediated antimicrobial defense (Figure 2G) (Di Meo et al., 2016; Zhang et al., 2016).

Annexin-Induced ROSs Are NADPH Oxidase-2 Dependent

Within cells, ROSs are generated by different cellular sources localized in the cytosol, in peroxisomes, at mitochondrial membranes and at the plasma membrane (Di Meo et al., 2016). The main source of ROSs in DCs and other phagocytes is the plasma-membrane-bound enzyme complex NADPH oxidase-2 (NOX-2), which catalyzes the formation of the superoxide radical O^{2-}, which is rapidly dismutated into hydrogen peroxide (H_2O_2) in the extra-cytosolic environment (Cachat et al., 2015; Di Meo et al., 2016). In a first attempt to characterize the source of annexin-induced ROSs, we aimed to scavenge extracellular

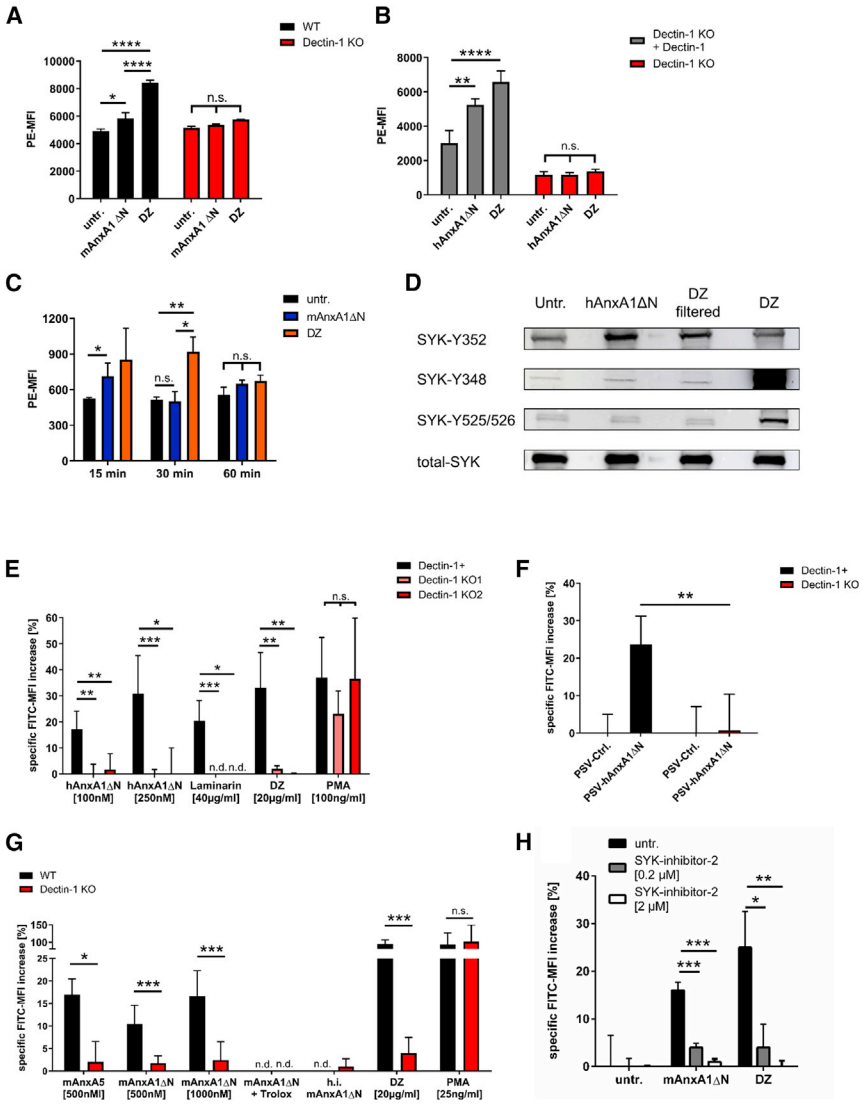

Figure 2. Annexin Induces SYK-Phosphorylation and Production of ROSs in a Dectin-1-Dependent Manner

(A–C) Spleen tyrosine kinase (SYK) phosphorylation in bone-marrow-derived DCs (BMDCs) (A) or human MM6 cells (B) was analyzed by flow cytometry. Cells were treated as indicated in the presence of the phosphatase inhibitor sodium vanadate (1 mM) (A and B) or without phosphatase inhibition in WT BMDCs (C) and stained intracellularly by an antibody against phosphorylated SYK (p-SYK) on Y348. PE-MFI, phycoerythrin median fluorescence intensity.

(D) Detection of p-SYK on Y348, Y352, and Y525/526. 5×10^5 Dectin-1-expressing MM6 cells were starved for 2 h in RPMI/1% FCS/0.1% oxaloacetate pyruvate insulin media supplement (OPI) and treated with indicated ligands in the presence of the phosphatase inhibitor sodium vanadate (1 mM) for 20 min. Lysates of 2.5×10^5 cells were loaded on a SDS gel and analyzed on western blot (WB) for the indicated p-SYK residues. Results are representative of three independent experiments.

(E–H) Intracellular ROS levels were determined by 2′,7′-dichlorodihydrofluorescein diacetate (H_2DCFDA) in MM6 cells (E and F) and in BMDCs (G and H). (H) 8 µg/mL DZ and 1,000 nM AnxA1ΔN were used. Phorbol 12-myristate 13-acetate (PMA) and the Dectin-1 ligands DZ and laminarin were used as positive controls. Co-treatment of annexin (Anx) A1ΔN with the ROS scavenger 6-hydroxy-2,5,7,8-tetramethylchroman-2-carboxylic acid (Trolox) as well as heat-inactivated (h.i.) AnxA1ΔN were used as negative controls. FITC-MFI, fluorescein isothiocyanate mean fluorescence intensity; PSV, PS-containing vesicles.

Results in (A)–(C) and (F) represent the mean ± SD of one representative experiment out of two or (H) one representative experiment out of three. In (E) and (G), the mean ± SD of three (mAnxA5, h.i. mAnxA1ΔN, DZ), four (mAnxA1ΔN + Trolox), eight (mAnxA1ΔN [500nM], PMA), or nine (mAnxA1ΔN [1000nM]) independent experiments are shown. ****$p < 0.0001$; ***$p < 0.001$; **$p < 0.01$; *$p < 0.05$; n.s., not significant; n.d., no FITC-MFI increase detected (unpaired, two-tailed t test). See also Figure S4.

H_2O_2 by using the membrane-impermeable enzyme catalase. Addition of catalase to the medium abrogated annexin-mediated ROS production (Figures 3A and S4G). Thus, we considered membrane-bound NOX enzymes as likely candidates for the source of annexin-mediated ROSs. To further clarify the involvement of NOX, we additionally used the nonspecific NOX inhibitor diphenyleneiodonium (DPI). As observed for catalase treatment, pretreatment with DPI blocked annexin-induced ROSs (Figures 3B and S4G).

Of all NOX isoforms, Dectin-1 stimulation by β-glucans has been particularly associated with activation of NOX-2 (Tam et al., 2014; Blanco-Menéndez et al., 2015). For specific targeting of NOX-2 in our assays, we used the peptide inhibitor *gp91-TAT* that competitively inhibits NOX-2 assembly, but not the activation of other NOX enzymes (Csányi et al., 2011). In agreement with a role for NOX-2 in annexin signaling, *gp91-TAT* significantly reduced annexin-induced ROS production compared to the control peptide *Scr-TAT* (Figures 3C and S4H). Consistent with this, the NOX-2-specific small-molecule inhibitor GSK2795039 also blocked annexin-induced ROSs (Figure 3D) (Hirano et al., 2015). Finally, we performed ROS experiments in BMDCs deficient for the main subunit of the NOX-2 complex, gp91 ($gp91^{phox(Y/X-)}$ male mice), and compared them with BMDCs from wild-type (WT) littermates. In line with our previous results, the ROS signal of annexin was dramatically reduced in NOX-2-deficient BMDCs (Figures 3F and S5A). However, stimulation by the NOX-independent ROS inducer rotenone remained unaffected (Figure S5B). Altogether, these experiments identify NOX-2 as a critical mediator of annexin-mediated ROS production after binding to Dectin-1.

Intriguingly, not all hallmarks of Dectin-1 signaling following stimulation by β-glucans were initiated by annexin A1ΔN. In contrast to Dectin-1-specific ligands such as DZ, annexin A1ΔN did not activate the transcription factor NF-κB or induce

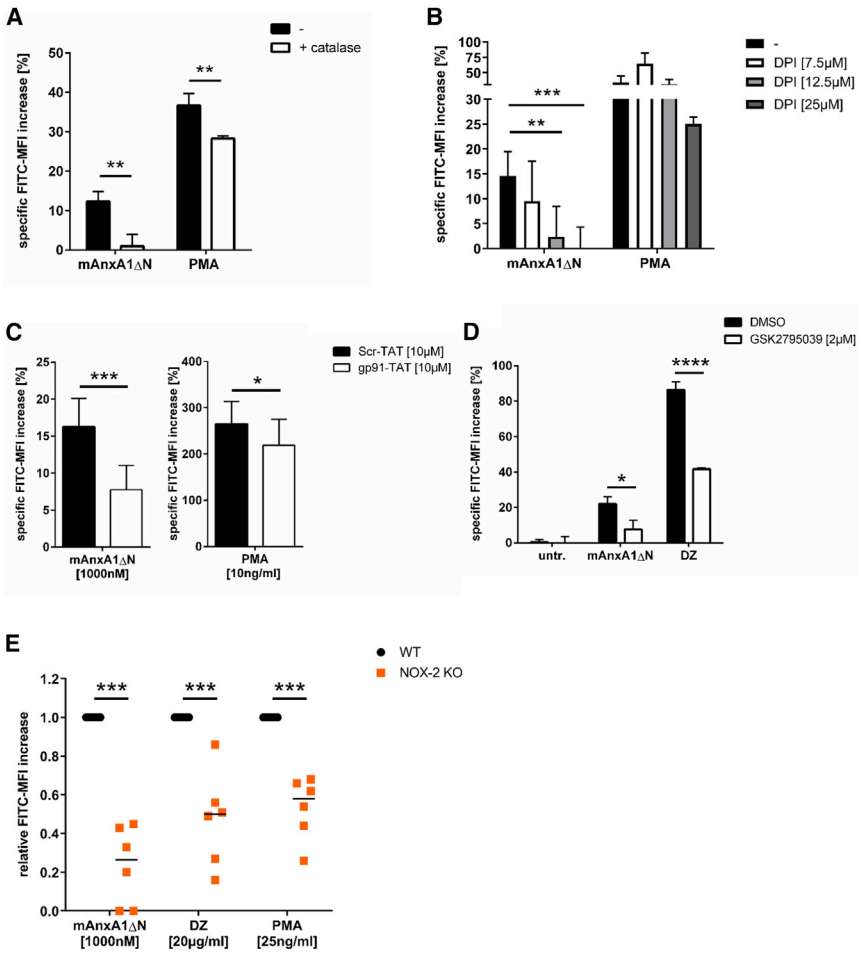

Figure 3. Annexin-Induced ROSs Are Derived from NADPH Oxidase-2

H_2DCFDA ROS detection experiments were performed as described in Figure 2.

(A–D) Dectin-1-expressing BMDCs were pre-incubated for 30–60 min with the indicated ROS scavenger before addition of the treatment. Results represent mean ± SD of at least two (B), three (D), or four (A and C) independent experiments. (E) BMDCs from NOX-2-deficient mice or WT littermates were treated with indicated ligands. Quantification of six independent experiments. The relative ROS-increase is normalized to untreated cells and the ROS-increase of WT control cells were set to 1 (WT BMDCs: black circles; NOX-2 KO BMDCs: orange squares). FITC, fluorescein isothiocyanate; MFI, mean fluorescence intensity. ***$p < 0.001$, **$p < 0.01$, *$p < 0.05$ (paired, two-tailed t test). Significant outliers (ρ values < 0.05) as determined by *GraphPad* outlier calculator were removed.

See also Figure S5.

inflammatory cytokine secretion (Figures 4A–4D). As described by Goodridge et al. (2011), extensive receptor clustering or formation of a synapse is required for activation of NF-κB and induction of cytokine secretion, respectively. In order to investigate Dectin-1 binding in the absence of extensive receptor clustering, we abrogated the ability of DZ to form large receptor/ligand clusters by filtering (0.45 μm). Indeed, such filtered, soluble DZ retained its ability to bind to Dectin-1 and induce ROS production, whereas we could not observe any activation of NF-κB or secretion of inflammatory cytokines (Figures 4E, 4F, and S3A; data not shown). These results imply that binding to Dectin-1 by ligands that do not induce extensive receptor clustering, such as the annexin core domain or soluble, filtered DZ, induce only selective Dectin-1 signaling events.

Dectin-1 Mediates Immunosuppressive Effects of ACs and Annexins

Externalization of annexins on ACs is critically involved in the induction of a tolerogenic DC-phenotype and the development of peripheral tolerance (Weyd, 2016). This immunosuppressive effect of ACs or annexins on DCs is illustrated by reduced responsiveness to Toll-like receptor (TLR) stimulation (Voll et al., 1997; Weyd et al., 2013). In the following experiments, we tested the role of Dectin-1 in immunosuppressive effects of ACs or the annexin core domain, respectively. As described before, ACs and annexin A1ΔN exerted a strong immunosuppressive effect on Dectin-1-expressing cells demonstrated by almost complete reduction (percentage of stimulation) of TLR-induced pro-inflammatory cytokine secretion (Weyd et al., 2013; Linke et al., 2015). In contrast, Dectin-1 KO cells were significantly less inhibited by both annexin A1ΔN and human as well as murine ACs (Figures 5A–5F and S6). Moreover, suppression of the co-stimulatory DC surface marker CD80 was prevented in Dectin-1 KO cells (Figures 5G and 5H). It is worth noting that the suppressive capacity of annexin A1ΔN was reduced in Dectin-1-deficient cells compared to WT cells in all corresponding experiments. Altogether, these data outline an important role for Dectin-1 as immunosuppressive receptor in response to ACs and the annexin A1 core domain.

Effective Immunosuppression by ACs and Annexins Requires ROSs

As shown above, annexin-mediated ROS production is abrogated by pretreatment with NOX-2-specific inhibitors or in NOX-2-deficient BMDCs, confirming that NOX-2 is the main ROS-producing enzyme after annexin incubation. Next to its well-known role in antimicrobial defense, NOX-2 has also described to be involved in anti-inflammatory processes as well as in prevention of autoimmune diseases (Olofsson et al., 2003; Rosenzweig, 2008; Lee et al., 2011; Holmdahl et al., 2013; Kelkka et al., 2014; Segal et al., 2010). Thus, we investigated whether annexin- and AC-induced immunosuppression was dependent on the induction of ROSs. Indeed, the H_2O_2-scavenger catalase reduced the suppressive effects of ACs and annexin compared to control-treated cells (Figures S7A–S7C). Accordingly, the suppressive effects of ACs and annexins were strongly reduced in functional

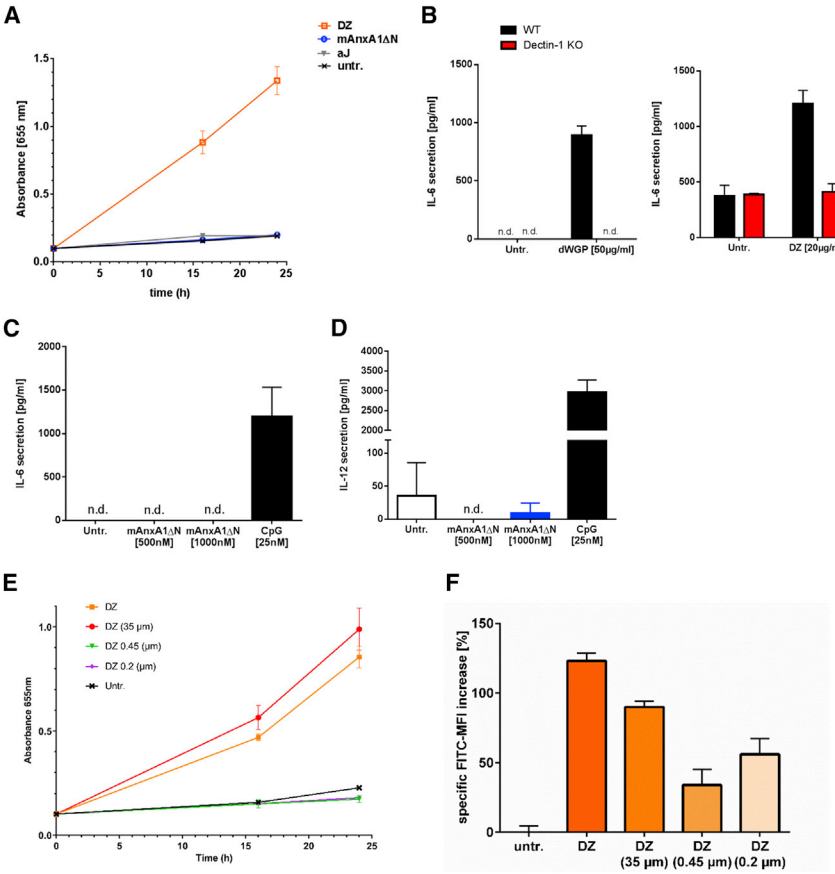

Figure 4. ACs, Recombinant AnxA1ΔN, and Filtered DZ Do Not Activate NF-κB

(A) Dectin-1 expressing NF-κB reporter cells (see STAR Methods) were treated with indicated ligands overnight. After 16h and 24h, activity of secreted embryonic alkaline phosphatase (SEAP) was assessed in the supernatant. Results indicate the mean ± SD of one representative experiment out of two.

(B) Dectin-1-deficient and WT BMDCs were incubated with indicated Dectin-1 agonists overnight. Cytokine concentrations in the supernatants were analyzed by ELISA 20-24 h after stimulation.

(C and D) WT BMDCs were stimulated with indicated treatment overnight. Cytokine concentrations in the supernatants were analyzed by ELISA 24 h after stimulation.

(E) Dectin-1-expressing NF-κB reporter cells were treated with indicated ligands overnight as described in (A).

(F) Intracellular ROS levels were determined by 2′,7′-dichlorodihydrofluorescein diacetate (H_2DCFDA) in WT BMDCs as described in Figure 2. Results represent the mean ± SD of one out of two independent experiments.

experiments using GSK2795039 (Figures 6A–6C and S7D–S7I) and *gp91-TAT* (Figures 6D–6G and S7J–S7Q) for inhibition of NOX-2. Finally, we confirmed the functional relationship between NOX-2-dependent ROS production and immunosuppression using gp91$^{phox(Y/X-)}$ BMDCs (Figures 6H–6K and S7R–S7U). We also observed significantly enhanced secretion of pro-inflammatory cytokines such as interleukin-6 (IL-6) and IL-12 in gp91$^{phox\ (Y/X-)}$ BMDCs after stimulation with a Dectin-1-specific β-glucan, confirming the inhibitory function of NOX-2-derived ROSs in Dectin-1-activated cells as described before (Figures S5C and S5D) (Schäppi et al., 2008; Segal et al., 2010).

Our data clearly show the relevance of NOX-2-induced ROSs for Dectin-1-mediated immunosuppression in response to the annexin core domain and ACs. Furthermore, the molecular mechanism of AC-mediated immunosuppression we have described here provides a rationale for the role of NOX-2 in regulating hyper-inflammatory immune responses and autoimmune diseases.

Dectin-1 KO Mice Show Age-Related Symptoms of Autoimmunity and Enhanced Immune Responses against AC-Derived Antigens

The *in vitro* results presented above delineate an immunoregulatory molecular pathway initiated by AC-bound annexin, which activates Dectin-1 and leads to DC-inhibition via phosphorylation of SYK followed by NOX-2-dependent ROS release. We anticipated that deficiency in either of these components would likely result in an autoimmune phenotype. Regarding NOX-2, it is well documented that mutations in members of the NOX-2 complex are responsible for a diverse set of autoimmune disorders, including rheumatoid arthritis or lupus erythematosus (Olofsson et al., 2003; Rosenzweig, 2008; Segal et al., 2010). However, Dectin-1-deficient mice have not been described to develop an overt autoimmune phenotype so far. We reasoned that autoimmune symptoms related to loss of Dectin-1 might accumulate with age as observed for other immune-regulators such as programmed cell death protein 1 (Nishimura et al., 1999) and thus investigated immune parameters in aged mice (77 weeks). We expected signs of hyper-inflammation in Dectin-1 KO mice due to a lack of sufficient DC and macrophage suppression during homeostatic turnover of engulfed ACs. Indeed, aged Dectin-1 KO mice showed severely enlarged spleens compared to WT littermates (Figure 7A). Moreover, DCs and macrophages in spleens of aged Dectin-1 KO mice displayed an activated phenotype as analyzed by CD80 or CD86 (co-)expression (Figures 7B–7E). Importantly, the activated cellular phenotype in aged Dectin-1 KO mice was accompanied by a higher titer of autoantibodies (immunoglobulin M [IgM] and IgG isotypes) targeting double-stranded DNA (Figures 7F–7H). In order to investigate the role of AC-mediated immune regulation in Dectin-1-deficient mice, we injected ACs stably expressing murine annexin A1 (mAnxA1) and the model antigen ovalbumin (OVA) into WT and Dectin-1 KO mice (Figure 7I). As depicted in Figure 7J, we observed a significant increase in OVA-specific $CD8^+$ T cells in draining lymph nodes of Dectin-1 KO mice compared to WT littermates. This observation indicates that Dectin-1-deficient mice lack immunosuppressive signaling when encountering ACs and thus mount stronger immune responses against AC-derived antigens (Figure 7J). In contrast to WT

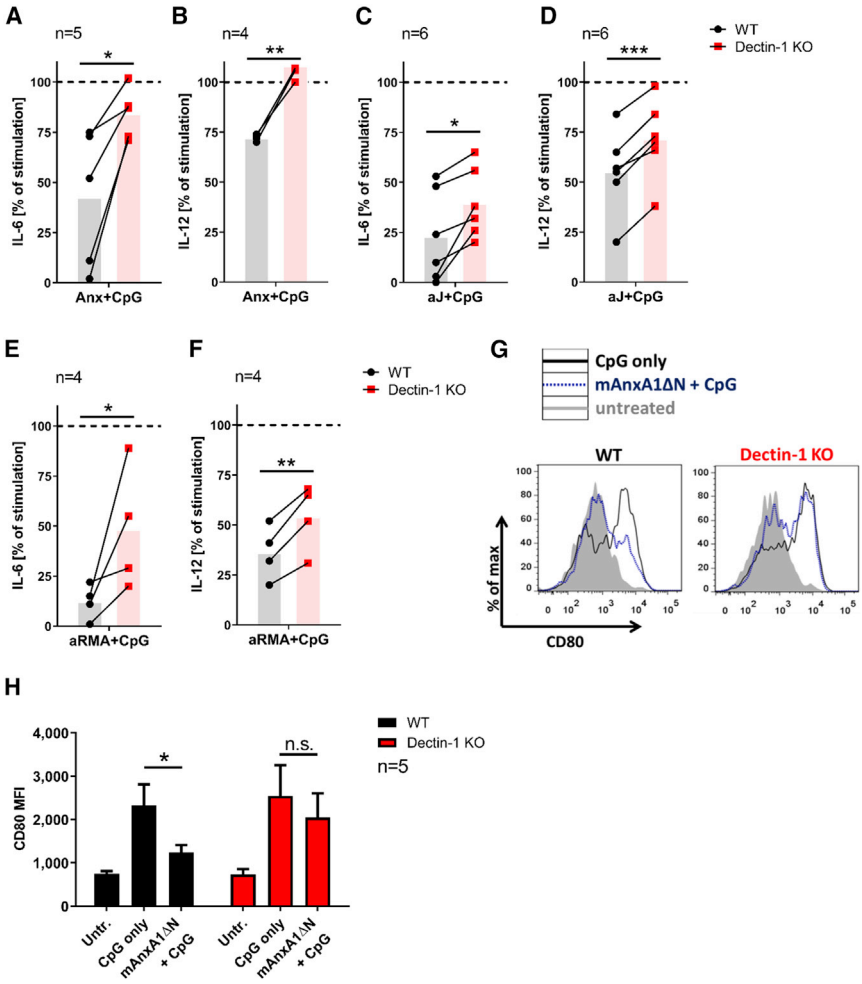

Figure 5. Dectin-1 Mediates Immunosuppressive Effects of ACs and Annexins

BMDCs were incubated with mouse (m) annexin (Anx) A1ΔN (1,000 nM), apoptotic Jurkat T cells (aJ; ratio of 0.5:1 or 0.1:1) or apoptotic RMA cells (aRMA; ratio of 4:1) for 8 h. After preincubation, BMDCs were stimulated over night with the TLR agonist CpG. Cytokine concentrations in the supernatants were analyzed by ELISA 16–24 h after stimulation (see representative experiments depicted as actual cytokine secretion in Figures S5A–S5P).

(A–F) Quantification of indicated independent experiments (n = 4–6). The cytokine secretion is normalized to CpG-stimulation minus background (100 − ((treated - untreated)/(CpG only − untreated)) × 100). The range of cytokine secretion was (A) 154–2,039 pg/mL, (B) 609–22,879 pg/mL, (C) 62–4,425 pg/mL, (D) 1,796–9,487 pg/mL, (E) 960–7,273 pg/mL, and (F) 7,513–19,413 pg/mL.

(G and H) CD80 surface staining was analyzed by flow cytometry after preincubation with eukaryotically expressed mAnxA1ΔN following simulation with CpG for 2–3 days.

(G) Representative histogram of CD80 expression in WT (left) and Dectin-1 KO BMDCs (right) with indicated treatments.

(H) Quantification of CD80 surface marker expression. Results represent the mean ± SEM of five independent experiments. ***$p < 0.001$; **$p < 0.01$; *$p < 0.05$ (paired, two-tailed t test).

See also Figure S6.

littermates, levels of the inflammatory biomarker soluble urokinase receptor (uPAR) as well anti-AC antibodies were also elevated in AC-injected Dectin-1-deficient mice (Figures 7K and 7L). Taken together, the autoimmune symptoms prevalent in aged Dectin-1 KO mice as well as stronger immune responses to AC-derived antigens in Dectin-1 KO mice demonstrate an involvement of Dectin-1 in homeostatic immune-regulation. Furthermore, this autoimmune phenotype *in vivo* supported by our *in vitro* studies reveals an important role for Dectin-1 in AC-mediated immunosuppression and in turn preventing the development of immune hyper-activation and autoimmunity.

DISCUSSION

Data presented in this study identify the CLR Dectin-1 as an immunosuppressive signaling receptor for annexins exposed on the surface of ACs. The fact that Dectin-1 and other CLRs bind endogenous ligands in addition to pathogen-derived ligands has been described before. Dectin-1 recognizes carbohydrate alterations as well as protein ligands, but the binding sites of endogenous protein ligands have not been investigated (Weck et al., 2008; Sancho and Reis e Sousa, 2013; Thiagarajan et al., 2013; Daley et al., 2017; Brown et al., 2018). Here, we show that the recognition site of the annexin core domain on Dectin-1 is distinct from its β-glucan-binding site. We determined a nanomolar affinity range of several annexin family members binding to Dectin-1, which compares well to the affinity of the inhibitory Dectin-1 ligand laminarin (Adams et al., 2008). Using QCM technology, we calculated an affinity for the soluble annexin A1 core domain and annexin A5 to Dectin-1-expressing cells of ~408 nM or ~7.1 nM, respectively (Table S1). This binding affinity was substantially increased when vesicle-bound annexin A1 core domain was applied to Dectin-1-expressing cells (data not shown). Because the annexin core domain is bound to PS on the surface of ACs under physiological conditions, this observation indicates a supportive role for PS binding that results in enhanced annexin A1/Dectin-1 interaction.

In line with the unique binding site mentioned above and in contrast to Dectin-1-dependent phagocytosis of β-glucans (Dambuza and Brown, 2015), we could not detect a prominent role for the Dectin-1/annexin interaction in phagocytosis or efferocytosis in BMDCs (data not shown), likely due to additional phagocytic receptors on BMDCs. A plethora of receptors has been described to be involved in the uptake of ACs (Arandjelovic and Ravichandran, 2015). In addition to PS receptors such as TREM-2, TIM-4, and CD300, lectin receptors binding to altered sugar residues presented on ACs or CD14 binding to AC-specific ICAM-3 may also be responsible for uptake of ACs in a highly redundant manner. According to our data, phagocytosis of ACs or annexin-loaded liposomes by BMDCs

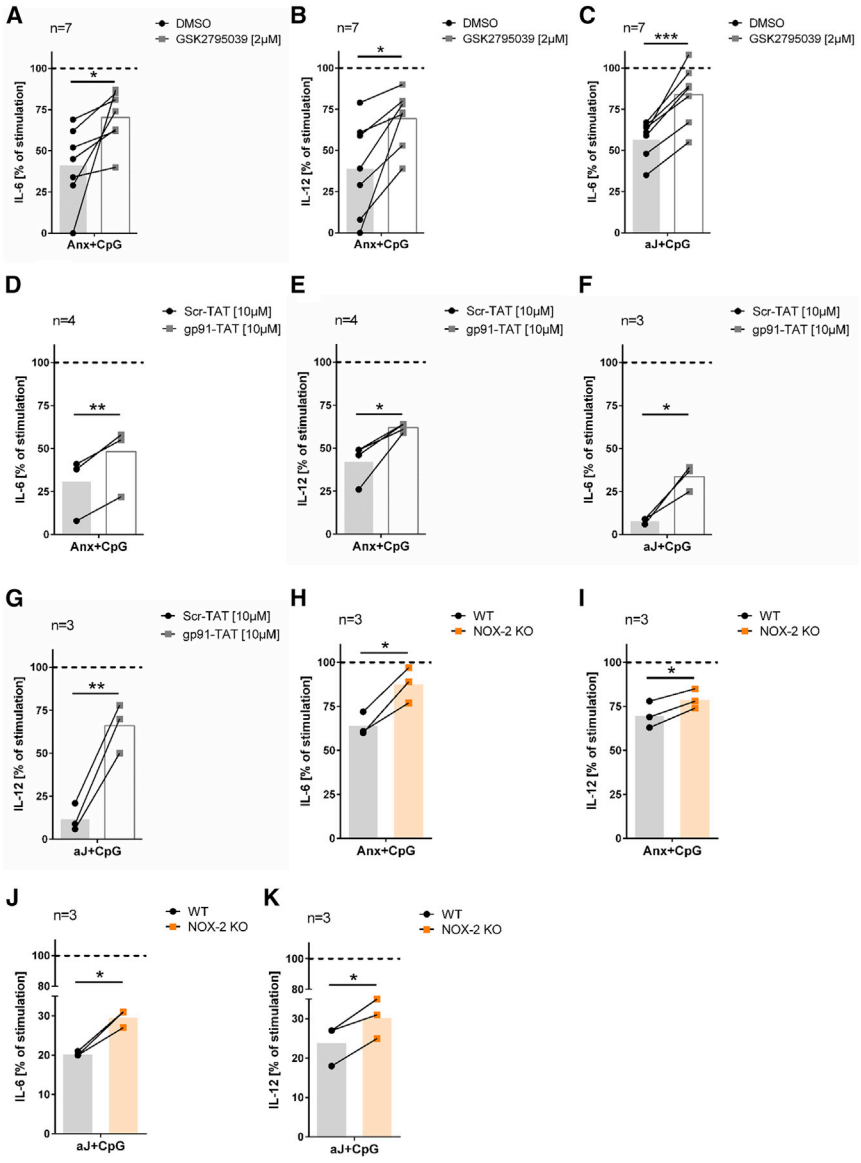

Figure 6. Effective Immunosuppression of AC-Derived Annexins Requires ROSs

(A–G) Quantification of suppression experiments performed as in Figure 5 for indicated cytokines. WT BMDCs were preincubated with NOX-2 inhibitors GSK2795039 (A–C) or gp91-TAT (D–G) for 30 min. Subsequently, apoptotic Jurkat T cells (aJ; ratio of 0.5:1) (C, F, and G) or eukaryotically expressed mAnxA1ΔN cells (1,000 nM) (A, B, D, and E) were added, and BMDCs were further incubated for 8 h.

(H–K) BMDCs generated from NOX-2-deficient mice and WT littermate controls were incubated with aJ cells (ratio of 2:1) (J and K) or mAnxA1ΔN (500 nM) (H and I). After preincubation, BMDCs were stimulated with the TLR agonist CpG. Indicated cytokines in the supernatants were analyzed by ELISA 20-24 h after stimulation.

The range of cytokine secretion was 75–3,746 pg/mL (A), 270–10,798 pg/mL (B), 745–4,298 pg/mL (C), 1,017–3,111 pg/mL (D), 4,197–6,832 pg/mL (E), 384–2,543 pg/mL (F), 2,153–8,465 pg/mL (G), 93–1,159 pg/mL (H), 438–3,540 pg/mL (I), 1,702–3,318 pg/mL (J), and 2,885–5,766 pg/mL (K). Results represent the means of three (F–K), four (D and E), or seven (A–C) independent experiments. ***$p < 0.001$; **$p < 0.01$; *$p < 0.05$ (paired, two-tailed t test).

See also Figure S7.

appears to be mediated mainly by phagocytic receptors other than Dectin-1.

Our results clearly show that the annexin A1 core domain and soluble, filtered β-glucans induce SYK-phosphorylation of Y348 and Y352 (Figure 2D). These residues are located within the SH2/SH3-linker of SYK required for binding and activation of PLCγ and ROS induction. Interestingly, Y525/526 within the SYK activation loop and important for NF-κB activation (Law et al., 1996) remained unphosphorylated (Figure 2D). In contrast, large particulate β-glucans induced prominent phosphorylation of all tyrosines investigated (Figure 2 D). Based on these results, we conclude that the annexin A1 core domain induces a distinct, non-canonical activation of Dectin-1 that is not dependent on extensive receptor clustering described for particulate β-glucans (Plato et al., 2013). Further observations support this conclusion. Soluble, filtered DZ mimics binding of the annexin A1 core domain to Dectin-1 and loses its ability to activate NF-κB or induce cytokine secretion, respectively (Figure 4E; data not shown), while selective SYK-phosphorylation and induction of ROS production is preserved (Figures 2D, S3A, and 4F).

Thus, the annexin A1 core domain selectively engages an anti-inflammatory branch of the Dectin-1 signaling pathway (Schäppi et al., 2008; Trinath et al., 2014). Such functional selectivity, also known as "biased agonism," has been described for other ligand/receptor systems (Smith et al., 2018). Selective activation of Dectin-1 by the annexin core domain induces a tolerogenic DC phenotype after phagocytosis of ACs and thus ensures the maintenance of peripheral immune tolerance.

Recognition of the annexin core domain by Dectin-1 leads to SYK-mediated induction of NOX-2-dependent release of ROSs that are known signaling events of many other Dectin-1 ligands (Tam et al., 2014; Blanco-Menéndez et al., 2015; Dambuza and Brown, 2015). However, annexin-induced intracellular ROS levels were substantially lower than the ROS levels characteristic of an oxidative burst, indicative of a role in signaling cascades (Zhang et al., 2016). The inhibitory function of NOX-2-derived ROSs is supported by publications describing NOX-2-derived ROSs as a factor in limiting hyper-inflammatory Dectin-1 responses (Schäppi et al., 2008; Segal et al., 2010). Moreover, it is known that NOX-2-derived ROSs play a substantial role in the prevention of autoimmune diseases in mice, rats, and

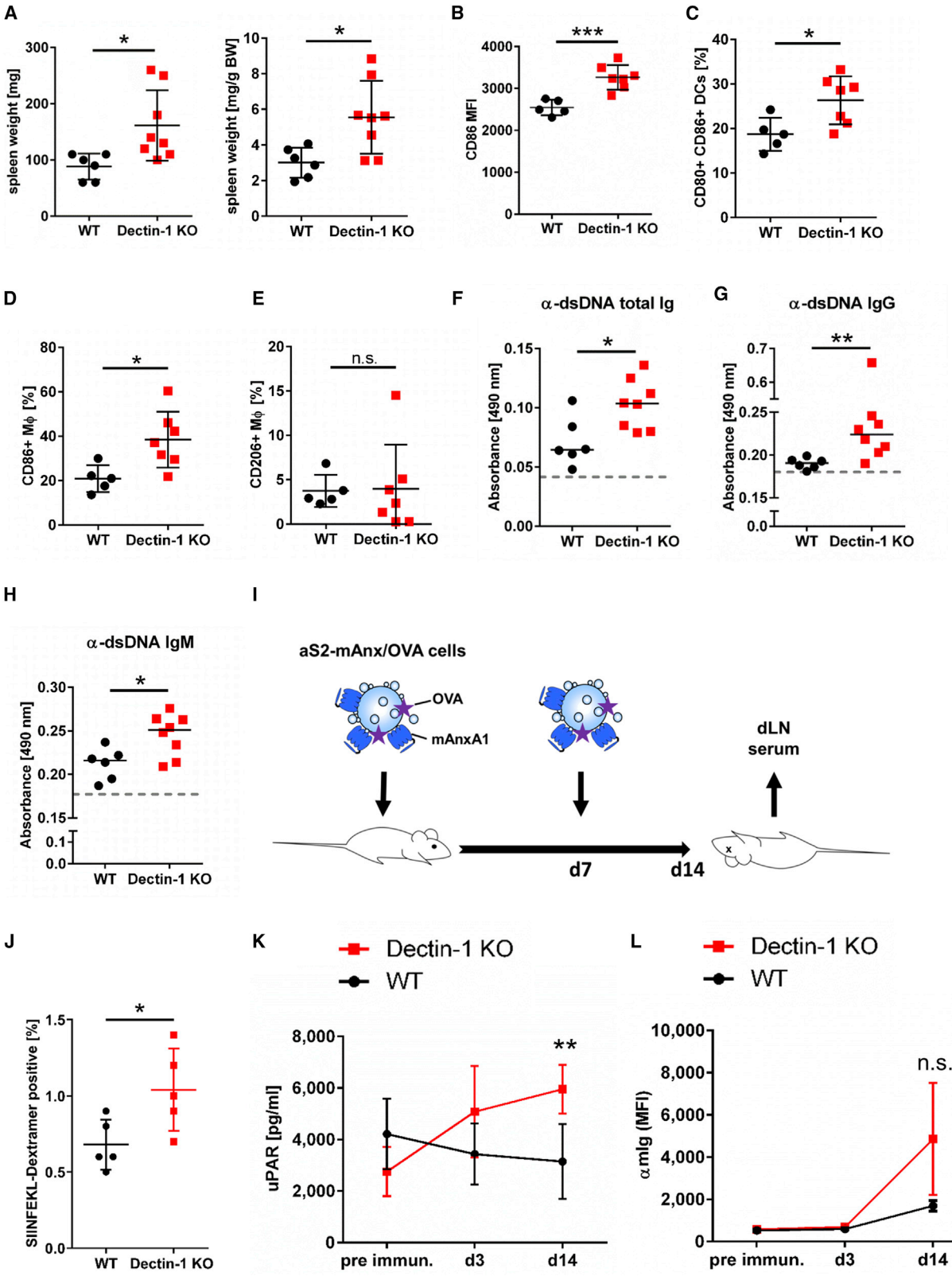

(legend on next page)

humans (Olofsson et al., 2003; Rosenzweig, 2008; Lee et al., 2011; Holmdahl et al., 2013; Kelkka et al., 2014; Segal et al., 2010).

The inhibitory role of the annexin/Dectin-1 axis was supported by data when testing immune responses against AC-derived antigens *in vivo*. Here, we observed an increase in AC-specific $CD8^+$ T cells in Dectin-1 KO mice compared to WT littermates accompanied by higher levels of uPAR and elevated anti-AC-specific antibodies in sera of AC-injected Dectin-1-deficient mice (Figure 7). The lack of inhibitory signaling in response to ACs apparent in Dectin-1-deficient mice also became evident in aged Dectin-1 KO mice. In fact, spleens of old Dectin-1 KO mice were enlarged and showed up to a 2-fold increase in weight. Moreover, an activated immune phenotype in aged Dectin-1 KO mice became evident by upregulation of activation markers on splenic DCs and macrophages. Importantly, these signs of immune activation in aged Dectin-1 KO mice were accompanied by elevated titers of anti-dsDNA autoantibodies. While Dectin-1-sufficient mice developed only IgM anti-dsDNA antibodies, in aged Dectin-1 KO mice, we observed an isotype switch toward anti-dsDNA IgG antibodies, which are known to closely correlate with disease onset and severity of autoimmune disorders such as systemic lupus erythematosus in humans (Förger et al., 2004). Our findings are supported by other studies that describe the induction of anti-inflammatory and tolerogenic responses upon Dectin-1 activation by β-glucans (Dillon et al., 2006; Karumuthil-Melethil et al., 2014, 2015).

We identified an essential role for NOX-2-derived ROSs in AC- and annexin-mediated DC-inhibition. In agreement with these findings, NOX-2-deficient mice develop an autoimmune phenotype with an onset at 5 weeks after birth that is characterized by arthritis- as well as lupus-like symptoms (Cachat et al., 2015; Lee et al., 2011). The pathologies in NOX-2-deficient mice appear to be more severe than the symptoms we observed in aged Dectin-1 KO mice. This difference is probably explained by the fact that AC- and annexin-mediated DC-inhibition was not completely abrogated in Dectin-1 KO BMDCs, suggesting that additional receptors known to signal via NOX-2 may contribute to this inhibitory mechanism. Nevertheless, we assume that Dectin-1 deficiency may result in a more severe autoimmune phenotype upon environmental challenges of the immune system (Cusick et al., 2012; Gour et al., 2018).

The molecular pathway of AC-derived annexin, stimulating Dectin-1 and inducing cellular inhibition of DCs via NOX-2-derived ROSs, represents an important mechanism of peripheral immune tolerance. Therapeutic manipulation of the annexin/Dectin-1/NOX-2 checkpoint system such as coupling autoantigens to the annexin A1 core domain may provide future strategies for treatment of autoimmune diseases.

STAR★METHODS

Detailed methods are provided in the online version of this paper and include the following:

- KEY RESOURCES TABLE
- LEAD CONTACT AND MATERIALS AVAILABILITY
- EXPERIMENTAL MODEL AND SUBJECT DETAILS
  - Mice
  - Cell Lines
- METHOD DETAILS
  - Preparation of Bone-Marrow–Derived Dendritic Cells
  - Flow Cytometry
  - Antibodies, ELISA, and Reagents
  - Transfections and CRISPR/Cas9-Mediated Genome-Editing
  - Generation and Purification of Recombinant Proteins
  - Preparation of Apoptotic Cells (ACs)
  - *In Vitro* Suppression-Assay with ACs or Recombinant Proteins
  - RNA Isolation and Quantitative RT-PCR
  - Detection of Reactive Oxygen Species (ROSs)
  - Annexin-Coated Vesicle Production
  - Attana Cell 200 Quartz Crystal Microbalance (QCM) Analysis
  - Production of the CLR-Fc Fusion Protein Library and ELISA Binding Experiments
  - Surface Plasmon Resonance (SPR) Analysis
  - *In Vivo* Experiments
- QUANTIFICATION AND STATISTICAL ANALYSIS
- DATA AND CODE AVAILABILITY

Figure 7. Dectin-1 KO Mice Exhibit Symptoms of Autoimmunity and Generate Enhanced Immune Responses to ACs

(A) Spleen weight of aged WT and Dectin-1 KO mice.

(B–E) Splenocytes only (B) or DCs ($CD11c^+$ and major histocompatibility complex class II [MHC class II]$^+$) (C) and macrophages (MΦ, $F4/80^+$, and MHC class II^+) (D and E) of isolated splenocytes were stained in combination with the activation markers CD80 and CD86 (C and D) as well as the anti-inflammatory M2-macrophage marker CD206 (E) and analyzed by flow cytometry. Results represent the mean ± SD of five to eight mice per group. ***$p < 0.01$; **$p < 0.01$; *$p < 0.05$; n.s., not significant (unpaired, two-tailed t test).

(F–H) Blood plasma of aged mice obtained from cardiocentesis were collected and analyzed for indicated autoantibodies against double-stranded DNA (dsDNA) by ELISA. Results represent the median of five to eight mice per group. **$p < 0.01$; *$p < 0.05$ (Mann-Whitney test).

(I–L) Dectin-1 KO mice and WT littermates were injected with apoptotic S2 cells (aS2 cells) stably expressing mAnxA1 and membrane-anchored ovalbumin (OVA; aS2-mAnxA1/OVA cells) on days 0 and 7.

(I) Schematic representation of the experiment.

(J) OVA-specific $CD8^+$ T cells of the draining lymph node (dLN) were stained with SIINFEKL dextramers.

(K) The serum level of soluble urokinase receptor (uPAR) was measured 1 day before the first injection (preimmunization [pre immun.]), 3 days after the first injection (d3), and 7 days after the second injection of aS2-mAnxA1/OVA cells (d14).

(L) Serum of WT and Dectin-1-deficient mice obtained from indicated time points was incubated with S2-mAnxA1/OVA cells and stained with PE-labeled α-mIg. Results represent the mean ± SD (J) and (K) or mean ± SEM (L) of 5 mice per group. **$p < 0.01$; *$p < 0.05$; n.s., not significant (unpaired, two-tailed t test). The dashed line in (F)–(H) represents the absorbance of the negative control casein only. WT: black circles; Dectin-1 KO: red squares. BW, body weight; MFI, mean fluorescence intensity.

SUPPLEMENTAL INFORMATION

Supplemental Information can be found online at https://doi.org/10.1016/j.celrep.2019.11.086.

ACKNOWLEDGMENTS

We thank J. Meßmer, S. Pfrang, W. Mueller, J. Steiner, R. Mölle, T. Machauer, M. Trapp, V. Neubauer, A. Hartley, S. Schmitt, and T. Feyerabend for technical support. We also thank G. Hämmerling (all German Cancer Research Center, Heidelberg, Germany), K. Gülow (University Hospital Regensburg, Germany), T. Aastrup, T. Bass (Attana AB, Stockholm, Sweden), and W. Nickel (Heidelberg University Biochemistry Center, Heidelberg, Germany) for critical discussions. We thank K. Remans and J. Flock (EMBL, Heidelberg, Germany) for production of recombinant mAnxA1ΔN in Sf9 insect cells. Moreover, we thank H. Sauter for excellent secretarial assistance. This work was supported by the German Federal Ministry of Education and Research VIP+ validation fund.

AUTHOR CONTRIBUTIONS

P.H.K., H.W., K.B., and V.J. contributed to the study design. F.B. and K.B. cloned and amplified plasmids and produced recombinant annexins. F.B. performed ion-exchange chromatography and confirmed LPS removal in all recombinant annexins. K.B. generated CRISPR/Cas9-mediated Dectin-1 KO cells and stable Dectin-1 (re-)transfected cells. B.L. contributed essential reagents. T.H., K.B., and S.Z. performed ELISA binding experiments. S.Z. performed SPR binding experiments and produced C-type lectin receptor (CLR) hFc fusion proteins. K.B. and V.J. prepared bone marrow of mice, and K.B. performed BMDC differentiation. K.B. produced annexin-loaded vesicles. D.P. performed QCM-based binding experiments. K.B., H.W., and C.L. performed phosphorylated SYK (p-SYK) detection experiments. K.B. and C.L. performed ROS detection experiments. T.H. performed NF-κB reporter assays. K.B. performed functional *in vitro* suppression assays. H.W. and K.B. performed *in vivo* analysis. K.B., H.W., and P.H.K. wrote the manuscript.

DECLARATION OF INTERESTS

The following patents are related to this work: WO2017211964A1, WO 2016/113022, and EP19156258.6.

Received: March 19, 2019
Revised: July 18, 2019
Accepted: November 20, 2019
Published: December 24, 2019

REFERENCES

Adams, E.L., Rice, P.J., Graves, B., Ensley, H.E., Yu, H., Brown, G.D., Gordon, S., Monteiro, M.A., Papp-Szabo, E., Lowman, D.W., et al. (2008). Differential high-affinity interaction of dectin-1 with natural or synthetic glucans is dependent upon primary structure and is influenced by polymer chain length and side-chain branching. J. Pharmacol. Exp. Ther. *325*, 115–123.

Arandjelovic, S., and Ravichandran, K.S. (2015). Phagocytosis of apoptotic cells in homeostasis. Nat. Immunol. *16*, 907–917.

Blanco-Menéndez, N., Del Fresno, C., Fernandes, S., Calvo, E., Conde-Garrosa, R., Kerr, W.G., and Sancho, D. (2015). SHIP-1 couples to the Dectin-1 hemITAM and selectively modulates reactive oxygen species production in dendritic cells in response to Candida albicans. J. Immunol. *195*, 4466–4478.

Blume, K.E., Soeroes, S., Waibel, M., Keppeler, H., Wesselborg, S., Herrmann, M., Schulze-Osthoff, K., and Lauber, K. (2009). Cell surface externalization of annexin A1 as a failsafe mechanism preventing inflammatory responses during secondary necrosis. J. Immunol. *183*, 8138–8147.

Brown, G.D., Willment, J.A., and Whitehead, L. (2018). C-type lectins in immunity and homeostasis. Nat. Rev. Immunol. *18*, 374–389.

Cachat, J., Deffert, C., Hugues, S., and Krause, K.H. (2015). Phagocyte NADPH oxidase and specific immunity. Clin. Sci. (Lond.) *128*, 635–648.

Callahan, M.K., Williamson, P., and Schlegel, R.A. (2000). Surface expression of phosphatidylserine on macrophages is required for phagocytosis of apoptotic thymocytes. Cell Death Differ. *7*, 645–653.

Callahan, M.K., Halleck, M.S., Krahling, S., Henderson, A.J., Williamson, P., and Schlegel, R.A. (2003). Phosphatidylserine expression and phagocytosis of apoptotic thymocytes during differentiation of monocytic cells. J. Leukoc. Biol. *74*, 846–856.

Csányi, G., Cifuentes-Pagano, E., Al Ghouleh, I., Ranayhossaini, D.J., Egaña, L., Lopes, L.R., Jackson, H.M., Kelley, E.E., and Pagano, P.J. (2011). Nox2 B-loop peptide, Nox2ds, specifically inhibits the NADPH oxidase Nox2. Free Radic. Biol. Med. *51*, 1116–1125.

Cusick, M.F., Libbey, J.E., and Fujinami, R.S. (2012). Molecular mimicry as a mechanism of autoimmune disease. Clin. Rev. Allergy Immunol. *42*, 102–111.

Daley, D., Mani, V.R., Mohan, N., Akkad, N., Ochi, A., Heindel, D.W., Lee, K.B., Zambirinis, C.P., Pandian, G.S.B., Savadkar, S., et al. (2017). Dectin 1 activation on macrophages by galectin 9 promotes pancreatic carcinoma and peritumoral immune tolerance. Nat. Med. *23*, 556–567.

Dambuza, I.M., and Brown, G.D. (2015). C-type lectins in immunity: recent developments. Curr. Opin. Immunol. *32*, 21–27.

Di Meo, S., Reed, T.T., Venditti, P., and Victor, V.M. (2016). Role of ROS and RNS sources in physiological and pathological conditions. Oxid. Med. Cell. Longev. *2016*, 1245049.

Dillon, S., Agrawal, S., Banerjee, K., Letterio, J., Denning, T.L., Oswald-Richter, K., Kasprowicz, D.J., Kellar, K., Pare, J., van Dyke, T., et al. (2006). Yeast zymosan, a stimulus for TLR2 and dectin-1, induces regulatory antigen-presenting cells and immunological tolerance. J. Clin. Invest. *116*, 916–928.

Förger, F., Matthias, T., Oppermann, M., Becker, H., and Helmke, K. (2004). Clinical significance of anti-dsDNA antibody isotypes: IgG/IgM ratio of anti-dsDNA antibodies as a prognostic marker for lupus nephritis. Lupus *13*, 36–44.

Gerke, V., and Moss, S.E. (2002). Annexins: from structure to function. Physiol. Rev. *82*, 331–371.

Goodridge, H.S., Reyes, C.N., Becker, C.A., Katsumoto, T.R., Ma, J., Wolf, A.J., Bose, N., Chan, A.S., Magee, A.S., Danielson, M.E., et al. (2011). Activation of the innate immune receptor Dectin-1 upon formation of a 'phagocytic synapse'. Nature *472*, 471–475.

Gour, N., Lajoie, S., Smole, U., White, M., Hu, D., Goddard, P., Huntsman, S., Eng, C., Mak, A., et al. (2018). Dysregulated invertebrate tropomyosin–dectin-1 interaction confers susceptibility to allergic diseases. Sci. Immunol *3*, eaam9841.

Hirano, K., Chen, W.S., Chueng, A.L., Dunne, A.A., Seredenina, T., Filippova, A., Ramachandran, S., Bridges, A., Chaudry, L., Pettman, G., et al. (2015). Discovery of GSK2795039, a novel small molecule NADPH oxidase 2 inhibitor. Antioxid. Redox. Signal *23*, 358–374.

Holmdahl, R., Sareila, O., Pizzolla, A., Winter, S., Hagert, C., Jaakkola, N., Kelkka, T., Olsson, L.M., Wing, K., and Bäckdahl, L. (2013). Hydrogen peroxide as an immunological transmitter regulating autoreactive T cells. Antioxid. Redox Signal. *18*, 1463–1474.

Karumuthil-Melethil, S., Gudi, R., Johnson, B.M., Perez, N., and Vasu, C. (2014). Fungal β-glucan, a Dectin-1 ligand, promotes protection from type 1 diabetes by inducing regulatory innate immune response. J. Immunol. *193*, 3308–3321.

Karumuthil-Melethil, S., Sofi, M.H., Gudi, R., Johnson, B.M., Perez, N., and Vasu, C. (2015). TLR2- and Dectin 1-associated innate immune response modulates T-cell response to pancreatic β-cell antigen and prevents type 1 diabetes. Diabetes *64*, 1341–1357.

Kelkka, T., Kienhöfer, D., Hoffmann, M., Linja, M., Wing, K., Sareila, O., Hultqvist, M., Laajala, E., Chen, Z., Vasconcelos, J., et al. (2014). Reactive oxygen species deficiency induces autoimmunity with type 1 interferon signature. Antioxid. Redox Signal. *21*, 2231–2245.

Law, C.L., Chandran, K.A., Sidorenko, S.P., and Clark, E.A. (1996). Phospholipase C-gamma1 interacts with conserved phosphotyrosyl residues in the linker region of Syk and is a substrate for Syk. Mol. Cell. Biol. *16*, 1305–1315.

Lee, K., Won, H.Y., Bae, M.A., Hong, J.H., and Hwang, E.S. (2011). Spontaneous and aging-dependent development of arthritis in NADPH oxidase 2 deficiency through altered differentiation of CD11b+ and Th/Treg cells. Proc. Natl. Acad. Sci. USA *108*, 9548–9553.

Linke, B., Abeler-Dörner, L., Jahndel, V., Kurz, A., Mahr, A., Pfrang, S., Linke, L., Krammer, P.H., and Weyd, H. (2015). The tolerogenic function of annexins on apoptotic cells is mediated by the annexin core domain. J. Immunol. *194*, 5233–5242.

Maglinao, M., Eriksson, M., Schlegel, M.K., Zimmermann, S., Johannssen, T., Götze, S., Seeberger, P.H., and Lepenies, B. (2014). A platform to screen for C-type lectin receptor-binding carbohydrates and their potential for cell-specific targeting and immune modulation. J. Control. Release *175*, 36–42.

Morelli, A.E., and Thomson, A.W. (2007). Tolerogenic dendritic cells and the quest for transplant tolerance. Nat. Rev. Immunol. *7*, 610–621.

Mueller, D.L. (2010). Mechanisms maintaining peripheral tolerance. Nat. Immunol. *11*, 21–27.

Nishimura, H., Nose, M., Hiai, H., Minato, N., and Honjo, T. (1999). Development of lupus-like autoimmune diseases by disruption of the PD-1 gene encoding an ITIM motif-carrying immunoreceptor. Immunity *11*, 141–151.

Olofsson, P., Holmberg, J., Tordsson, J., Lu, S., Akerström, B., and Holmdahl, R. (2003). Positional identification of Ncf1 as a gene that regulates arthritis severity in rats. Nat. Genet. *33*, 25–32.

Peiris, D., Spector, A.F., Lomax-Browne, H., Azimi, T., Ramesh, B., Loizidou, M., Welch, H., and Dwek, M.V. (2017). Cellular glycosylation affects Herceptin binding and sensitivity of breast cancer cells to doxorubicin and growth factors. Sci. Rep. *7*, 43006.

Perretti, M., and Dalli, J. (2009). Exploiting the Annexin A1 pathway for the development of novel anti-inflammatory therapeutics. Br. J. Pharmacol. *158*, 936–946.

Perretti, M., Getting, S.J., Solito, E., Murphy, P.M., and Gao, J.L. (2001). Involvement of the receptor for formylated peptides in the in vivo anti-migratory actions of annexin 1 and its mimetics. Am. J. Pathol. *158*, 1969–1973.

Plato, A., Willment, J.A., and Brown, G.D. (2013). C-type lectin-like receptors of the dectin-1 cluster: ligands and signaling pathways. Int. Rev. Immunol. *32*, 134–156.

Pollock, J.D., Williams, D.A., Gifford, M.A., Li, L.L., Du, X., Fisherman, J., Orkin, S.H., Doerschuk, C.M., and Dinauer, M.C. (1995). Mouse model of X-linked chronic granulomatous disease, an inherited defect in phagocyte superoxide production. Nat. Genet. *9*, 202–209.

Pupjalis, D., Goetsch, J., Kottas, D.J., Gerke, V., and Rescher, U. (2011). nnexin A1 released from apoptotic cells acts through formyl peptide receptors to dampen inflammatory monocyte activation via JAK/STAT/SOCS signalling. EMBO Mol. Med. *3*, 102–114.

Ran, F.A., Hsu, P.D., Wright, J., Agarwala, V., Scott, D.A., and Zhang, F. (2013). Genome engineering using the CRISPR-Cas9 system. Nat. Protoc. *8*, 2281–2308.

Reid, D.M., Gow, N.A.R., and Brown, G.D. (2009). Pattern recognition: recent insights from Dectin-1. Curr. Opin. Immunol. *21*, 30–37.

Rosenzweig, S.D. (2008). Inflammatory manifestations in chronic granulomatous disease (CGD). J. Clin. Immunol. *28* (*Suppl 1*), S67–S72.

Salanti, A., Clausen, T.M., Agerbæk, M.Ø., Al Nakouzi, N., Dahlbäck, M., Oo, H.Z., Lee, S., Gustavsson, T., Rich, J.R., Hedberg, B.J., et al. (2015). Targeting human cancer by a glycosaminoglycan binding malaria protein. Cancer Cell *28*, 500–514.

Sancho, D., and Reis e Sousa, C. (2013). Sensing of cell death by myeloid C-type lectin receptors. Curr. Opin. Immunol. *25*, 46–52.

Schäppi, M., Deffert, C., Fiette, L., Gavazzi, G., Herrmann, F., Belli, D., and Krause, K.H. (2008). Branched fungal β-glucan causes hyperinflammation and necrosis in phagocyte NADPH oxidase-deficient mice. J. Pathol. *214*, 434–444.

Schneider, U., Schwenk, H.U., and Bornkamm, G. (1977). Characterization of EBV-genome negative "null" and "T" cell lines derived from children with acute lymphoblastic leukemia and leukemic transformed non-Hodgkin lymphoma. Int. J. Cancer *19*, 621–626.

Segal, B.H., Han, W., Bushey, J.J., Joo, M., Bhatti, Z., Feminella, J., Dennis, C.G., Vethanayagam, R.R., Yull, F.E., Capitano, M., et al. (2010). NADPH oxidase limits innate immune responses in the lungs in mice. PLoS ONE *5*, e9631.

Smith, J.S., Lefkowitz, R.J., and Rajagopal, S. (2018). Biased signalling: from simple switches to allosteric microprocessors. Nat. Rev. Drug Discov. *17*, 243–260.

Stolt-Bergner, P., Benda, C., Bergbrede, T., Besir, H., Celie, P.H.N., Chang, C., Drechsel, D., Fischer, A., Geerlof, A., Giabbai, B., et al. (2018). Baculovirus-driven protein expression in insect cells: A benchmarking study. J. Struct. Biol. *203*, 71–80.

Tam, J.M., Mansour, M.K., Khan, N.S., Seward, M., Puranam, S., Tanne, A., Sokolovska, A., Becker, C.E., Acharya, M., Baird, M.A., et al. (2014). Dectin-1-dependent LC3 recruitment to phagosomes enhances fungicidal activity in macrophages. J. Infect. Dis. *210*, 1844–1854.

Tanaka, M., Miyake, Y., and Asano, K. (2008). Maintenance of self-tolerance by apoptotic cell clearance. Front. Biosci. *13*, 6043–6049.

Taylor, P.R., Tsoni, S.V., Willment, J.A., Dennehy, K.M., Rosas, M., Findon, H., Haynes, K., Steele, C., Botto, M., Gordon, S., and Brown, G.D. (2007). Dectin-1 is required for beta-glucan recognition and control of fungal infection. Nat. Immunol. *8*, 31–38.

Temmerman, K., and Nickel, W. (2009). A novel flow cytometric assay to quantify interactions between proteins and membrane lipids. J. Lipid Res. *50*, 1245–1254.

Thiagarajan, P.S., Yakubenko, V.P., Elsori, D.H., Yadav, S.P., Willard, B., Tan, C.D., Rodriguez, E.R., Febbraio, M., and Cathcart, M.K. (2013). Vimentin is an endogenous ligand for the pattern recognition receptor Dectin-1. Cardiovasc. Res. *99*, 494–504.

Tiwari, N., Garbi, N., Reinheckel, T., Moldenhauer, G., Hämmerling, G.J., and Momburg, F. (2007). A transporter associated with antigen-processing independent vacuolar pathway for the MHC class I-mediated presentation of endogenous transmembrane proteins. J. Immunol. *178*, 7932–7942.

Trinath, J., et al. (2014). The WNT signaling pathway contributes to Dectin-1-dependent inhibition of toll-like receptor-induced inflammatory signature. Mol. Cell Biol *34*, 4301–4314.

Vaux, D.L., and Korsmeyer, S.J. (1999). Cell death in development. Cell *96*, 245–254.

Voll, R.E., Herrmann, M., Roth, E.A., Stach, C., Kalden, J.R., and Girkontaite, I. (1997). Immunosuppressive effects of apoptotic cells. Nature *390*, 350–351.

Walther, A., Riehemann, K., and Gerke, V. (2000). A novel ligand of the formyl peptide receptor: annexin I regulates neutrophil extravasation by interacting with the FPR. Mol. Cell *5*, 831–840.

Weck, M.M., Appel, S., Werth, D., Sinzger, C., Bringmann, A., Grünebach, F., and Brossart, P. (2008). hDectin-1 is involved in uptake and cross-presentation of cellular antigens. Blood *111*, 4264–4272.

Weyd, H. (2016). More than just innate affairs: on the role of annexins in adaptive immunity. Biol. Chem. *397*, 1017–1029.

Weyd, H., Abeler-Dörner, L., Linke, B., Mahr, A., Jahndel, V., Pfrang, S., Schnölzer, M., Falk, C.S., and Krammer, P.H. (2013). Annexin A1 on the surface of early apoptotic cells suppresses CD8+ T cell immunity. PLoS ONE *8*, e62449.

Yang, Y., Hutchinson, P., and Morand, E.F. (1999). Inhibitory effect of annexin I on synovial inflammation in rat adjuvant arthritis. Arthritis Rheum. *42*, 1538–1544.

Zhang, J., Wang, X., Vikash, V., Ye, Q., Wu, D., Liu, Y., and Dong, W. (2016). ROS and ROS-mediated cellular signaling. Oxid. Med. Cell. Longev. *2016*, 4350965.

Ziegler-Heitbrock, H.W., Thiel, E., Fütterer, A., Herzog, V., Wirtz, A., and Riethmüller, G. (1988). Establishment of a human cell line (Mono Mac 6) with characteristics of mature monocytes. Int. J. Cancer *41*, 456–461.

STAR★METHODS

KEY RESOURCES TABLE

REAGENT or RESOURCE	SOURCE	IDENTIFIER
Antibodies		
Monoclonal anti-mouse CD86-APC-Cy7	BioLegend	Cat# 105029; RRID: AB_2074993
Monoclonal anti-mouse CD11c-APC	BioLegend	Cat# 117309; RRID: AB_313778
Monoclonal anti-mouse H-2Kb/H-2Db-PerCP/Cy5.5	BioLegend	Cat# 114620; RRID: AB_2750200
Monoclonal anti-mouse F4/80-APC-Cy7	BioLegend	Cat# 123117; RRID: AB_893489
Monoclonal anti-mouse CD80-FITC	BioLegend	Cat# 104706; RRID: AB_313127
Monoclonal anti-mouse PD-L1–PE	BioLegend	Cat# 155404; RRID: AB_2728223
Monoclonal anti-mouse Dec205-PE-Cy7	BioLegend	Cat# 138209; RRID: AB_10643580
Monoclonal anti-p-SYK-PE (clone moch1ct)	eBioscience	Cat# 12-9014-42; RRID: AB_2572675
Monoclonal anti-hSYK-APC (clone 4D10.1)	LIFE Technologies	Cat# 17669641; RRID: AB_10717253
Monoclonal anti-human Dectin-1-PE (clone 15E2)	eBioscience	Cat# 12-9856-42; RRID: AB_2572749
Monoclonal anti-mouse CD11b-PE	Caltag	Cat# FP10116510; RRID: AB_2784511
Monoclonal anti-mouse CD80-PE	BD Biosciences	Cat# 553769; RRID: AB_395039
Monoclonal anti-mouse Dectin-1-FITC	Abcam	Cat# ab21646; RRID: AB_446449
Monoclonal anti-human AnxA1 (clone DAC5)	DKFZ, Heidelberg, Germany, Dr. H. Weyd	RRID: AB_2784513
Monoclonal anti-mouse AnxA1 (clone mAx550)	DKFZ, Heidelberg, Germany, Dr. H. Weyd	RRID: AB_2784514
Goat anti-mouse IgM, μ Chain Specific antibody	Jackson ImmunoResearch Labs	Cat# 115-001-020; RRID: AB_2338446
Goat anti-mouse IgG1	SouthernBiotech	Cat# 1070-05; RRID: AB_2650509
Goat anti-mouse IgG2b	SouthernBiotech	Cat# 1090-09; RRID: AB_2756437
Goat F(ab')2 anti-mouse IgG3	SouthernBiotech	Cat# 1102-09; RRID: AB_2784525
Goat anti-mouse IgG2c	Abcam	Cat# ab97255; RRID: AB_10680258
Anti-mouse Ig	Thermo Fisher Scientific	Cat# PA1-86023; RRID: AB_934405
Anti-human IgG-HRP	Dianova	Cat# 109-035-088; RRID: AB_2784521
Alkaline phosphatase-conjugated goat anti-human Fc	Dianova	Cat# GtxHu-004-EALP; RRID: AB_2784522
Anti-Syk Antibody, Unconjugated	Cell Signaling Technologies	Cat# 2712; RRID: AB_2197223
Polyclonal rabbit anti-human p-SYK (Tyr348)	Abcam	Cat# ab52212; RRID: AB_882779
Polyclonal rabbit anti-human p-SYK (Tyr352)/ ZAP70 (Tyr319)	Cell Signaling Technologies	Cat# #2701T; RRID: AB_331600
Polyclonal rabbit anti-human p-SYK (Tyr525/526)	Cell Signaling Technologies	Cat# 2711; RRID: AB_2197215
Bacterial and Virus Strains		
Escherichia coli strain Rosetta (DE3)	Novagen	Cat# 70954
Chemicals, Peptides, and Recombinant Proteins		
AnxA5-FITC (for detection of PS exposure)	Immunotools	Cat# 31490013
AnxA5-APC (for detection of PS exposure)	Immunotools	Cat# 31490016
hAnxA5 (for QCM binding experiments)	*Biotrend Chemikalien GmbH*	Cat# ATGP0406-500
mAnxA1 full length (procaryotically expressed)	DKFZ, Heidelberg, Germany, Weyd et al., 2013 and Linke et al., 2015	N/A

(*Continued on next page*)

Continued

REAGENT or RESOURCE	SOURCE	IDENTIFIER
mAnxA1ΔN (procaryotically expressed)	DKFZ, Heidelberg, Germany, Linke et al., 2015	N/A
mAnxA1ΔN (eukaryotically expressed)	EMBL, Heidelberg, Germany, this paper	N/A
mAnxA5 (procaryotically expressed)	DKFZ, Heidelberg, Germany, Linke et al., 2015	N/A
mAnxA13 (procaryotically expressed)	DKFZ, Heidelberg, Germany, Linke et al., 2015	N/A
7-aminoactinomycin D	Sigma-Aldrich	Cat# 7240-37-1
Sodium orthovanadate	Sigma-Aldrich	Cat# 13721-39-6
Laminarin	Invivogen	Cat# tlrl-lam
dWGP	Invivogen	Cat# tlrl-wgp
DZ	Invivogen	Cat# tlrl-zyd
BGP	Invivogen	Cat# tlrl-bgp
Bovine extracted catalase	Carl Roth	Cat# 6025.1
Trolox	Th. Geyer	Cat# CAY10011659-250
sgp91 ds - tat, scrambled	Anaspc	Cat# AS-63821
gp91 ds - tat	Anaspc	Cat# AS-63818
GSK2795039	MedChem Express	Cat# HY-18950
Collagenase Typ IV	Biochrome	Cat# C 4-28
DNase I	Roche	Cat# 10104159001
RPMI 1640	Sigma-Aldrich	Cat# R8758-500ML
FCS	Sigma-Aldrich	Cat# 12133C-500ML
2-Mercaptoethanol	Sigma-Aldrich	Cat# M6250
OPI-supplement	Sigma-Aldrich	Cat# O5003
Geneticin sulfate	GERBU Biotechnik	Cat# 1103,0250
Triton X-114	Sigma-Aldrich	Cat# X114
Blasticidin S Hydrochloride	Thermo Fisher Scientific	Cat# R21001
Hygromycin B	Gerbu	Cat# 1312,1
Penicillin-Streptomycin	Sigma-Aldrich	Cat# P4333
Polymyxin B sulfate salt	Sigma-Aldrich	Cat# P4932
CpG ODN 1668 - TLR9 ligand	Invivogen	Cat# tlrl-1668
R848 (Resiquimod)	Invivogen	Cat# tlrl-r848-5
SYBR® Green I nucleic acid gel stain	Sigma-Aldrich	Cat# S9430
H_2DCFDA	Sigma-Aldrich	Cat# D6883
NAC	Sigma-Aldrich	Cat# A7250
PC	Avanti Lipids Polar	Cat# 850375
PS	Avanti Lipids Polar	Cat# 840035
Cy5-PE	Avanti Lipids Polar	Cat# 810335
Chloroform	Sigma-Aldrich	Cat# C2432
EndoFit Ovalbumin	Invivogen	Cat# vac-pova
DPBS^{2+}	Sigma-Aldrich	Cat# D8662
Sucrose	Merck	Cat# S8501
GIBCO PBS, pH 7.4	Thermo Fisher Scientific	Cat# 11503387
4% formaldehyde, methanol-free	Thermo Fisher Scientific	Cat# FB002
DAPI	Merck	Cat# 1246530100
AMV Reverse Transcriptase	New England Biolabs	Cat# M0277S
p-nitrophenyl phosphate	Thermo Fisher Scientific	Cat# 34045
SYK-inhibitor-2	Merck	Cat# 574712-1MG

(*Continued on next page*)

Continued

REAGENT or RESOURCE	SOURCE	IDENTIFIER
MHC Dextramers/PE - H-2Kb/SIINFEKL	Immudex	Cat# JD2163
C-type lectin receptor Fc fusion protein library	Maglinao et al., 2014	N/A
mDectin-1 Fc	Invivogen	Cat# fc-mdec1a
o-Phenylenediamine	Thermo Fisher Scientific	Cat# 34005
Critical Commercial Assays		
Mouse IL-12p40 ELISA	PeproTech	Cat# 900-K97
Mouse IL-6 ELISA	BD Biosciences	Cat# 555240
Human TNFα ELISA	BD Biosciences	Cat# 555212
Anti-ds DNA ELISA	This paper	N/A
Limulus amoebocyte lysate assay	Lonza	Cat# 50-647U
AMAXA Cell Line Nucleofector Kit V	Lonza	Cat# VVCA-1003
RNeasy Mini Kit	QIAGEN	Cat# 74104
RNAqueous-Micro Total RNA Isolation Kit	Ambion	Cat# AM1931
Amplex Red Hydrogen Peroxide/ Peroxidase Assay Kit	Invitrogen	Cat# A22188
Attana amine coupling kit	Attana AB, Peiris et al., 2017	N/A
Amine Coupling Kit	GE Healthcare	Cat# BR100050
Mouse uPAR PicoKine ELISA Kit	Hölzel Diagnostika	Cat# BOS-EK1215
Experimental Models: Cell Lines		
Jurkat E6.1	Schneider et al., 1977	CVCL_0367
MM6	Ziegler-Heitbrock et al., 1988	CVCL_1426
hDectin-1b-expressing HEK293 NF-κB reporter cell-system	Invivogen	CVCL_VV20
RMA-OVA	Dr. G. Haemmerling, DKFZ, Heidelberg, Germany, Tiwari et al., 2007	N/A
Drosophila melanogaster S2 cells expressing mAnxA1 and membrane-anchored OVA	Linke et al., 2015	N/A
FreeStyle Max CHO-S Expression System	Thermo Fisher Scientific	Cat# K900020
Experimental Models: Organisms/Strains		
Mouse: B6.129S6-*Clec7a*^{tm1Gdb}/J	The Jackson Laboratory, Taylor et al., 2007	IMSR_JAX:012337
Mouse: B6.129S-*Cybb*^{tm1Din}/J	Dr. Vincent Jaquet, University of Geneva, Switzerland	IMSR_JAX:002365
Mouse: C57BL/6J	The Jackson Laboratory	IMSR_JAX:000664
Oligonucleotides		
gRNA#1 targeting Dectin-1 Exon 1: AACTTGTTTCACGCTATATC	This paper	N/A
gRNA#2 targeting Dectin-1 Exon 1: AAGATGTGCTTCGAGATGTG	This paper	N/A
Primer for Dectin-1 forward: AGACTCATCTGCTATGCTGCC	This paper	N/A
Primer for Dectin-1 reverse: AACGGGAGAGCTAAAGGCAC	This paper	N/A
Seq Primer for Dectin-1: GTCAGCAGTCTCAGAAACAGGA	This paper	N/A
qPCR Primer for hHPRT1 forward: TGACACTGGCAAAACAATGCA	This paper	N/A
qPCR Primer for hHPRT1 reverse: CCTACAGACCAGTTAGCGCACATC	This paper	N/A

(*Continued on next page*)

Continued

REAGENT or RESOURCE	SOURCE	IDENTIFIER
qPCR Primer for mHMBS forward: GAGTCTAGATGGCTCAGATAGCATGC	This paper	N/A
qPCR Primer for mHMBS reverse: CCTACAGACCAGTTAGCGCACATC	This paper	N/A
qPCR Primer for mDectin-1 A2 forward: GGGTGCCCTAGGAGGTTTTT	This paper	N/A
qPCR Primer for mDectin-1 A2 reverse: ACGGTGAGACGATGTTTGGC	This paper	N/A
qPCR Primer for hDectin-1 forward: TTGGCGCCTCATTGCTGTAA	This paper	N/A
qPCR Primer for hDectin-1 reverse: GGAGGACAAGGGCTGGAAAG	This paper	N/A
qPCR Primer for NOX-2 forward: TGTCCAAGCTGGAGTGGCACC	This paper	N/A
qPCR Primer for NOX-2 reverse: GTCCAGTCCCCAACGATGCGG	This paper	N/A
Recombinant DNA		
Plasmid: mAnxA1 full length for production in bacteria	Linke et al., 2015	N/A
Plasmid: mAnxA1ΔN for production in bacteria	Linke et al., 2015	N/A
Plasmid: mAnxA1ΔN for production in Sf9 insect cells	This paper	N/A
Plasmid: hAnxA1ΔN for production in bacteria	Linke et al., 2015	N/A
Plasmid: mAnxA5 for production in bacteria	Linke et al., 2015	N/A
Plasmid: mAnxA13 for production in bacteria	Linke et al., 2015	N/A
Plasmid: hDectin-1b	Invivogen	Cat# puno1-hdectin1b
Plasmid: pSpCas9(BB)-2A-GFP Vector	Ran et al., 2013	Addgene_48138
Plasmid: pFUSE-hIgG1-Fc	Invivogen	Cat# pfuse-hg1fc1
Software and Algorithms		
Graph Pad Prism (version 6)	PrismGraphPad Software Inc.	SCR_002798
FlowJo (version 7.6.5)	BD Biosciences	SCR_008520
Attester software	Attana AB, Peiris et al., 2017	N/A
Evaluation software	Attana AB, Peiris et al., 2017	N/A
TraceDrawer software	Ridgeview Instruments, Peiris et al., 2017	N/A
Biacore T100 Evaluation software	GE Healthcare, Maglinao et al., 2014	N/A
Biacore T100 Control software	GE Healthcare, Maglinao et al., 2014	N/A
Other		
Stratalinker 1800	Stratagene/Agilent Technologies	Cat# 99901-610
ABI Prism 7500 sequence detector system	Applied Biosystems	Cat# 4351107
Concentrator 5301	Eppendorf	Cat# 5305000100
SONOPULS HD 2070	Bandelin	Cat# HD 2070
Attana Cell 200 quartz crystal microbalance (QCM)	Attana AB, Peiris et al., 2017	N/A
Attana Cell 200 biosensor	Attana AB, Peiris et al., 2017	N/A
Biacore T100 instrument	GE Healthcare, Maglinao et al., 2014	Cat# GEBIACORET100SPR020215

LEAD CONTACT AND MATERIALS AVAILABILITY

Further information and requests for resources and reagents should be directed to and will be fulfilled by the Lead Contact, Peter H. Krammer (p.krammer@dkfz-heidelberg.de) with a completed Materials Transfer Agreement. We are glad to share all reagents with compensation by requestor for shipping. Stocks from recombinant annexins may need to be re-produced. Bone marrow (BM) of gp91$^{phox\ (Y/X-)}$ KO (B6.129S-Cybb$^{tm1Din/J}$) and gp91$^{phox\ (Y/X+)}$ WT male mice was kindly provided by V. Jaquet (University of Geneva, Geneva, Switzerland). The pCas9_GFP plasmid was a gift from Kiran Musunuru (Addgene plasmid # 44719). The OVA-expressing RMA cell line was a gift from G. Hämmerling (DKFZ, Heidelberg, Germany).

EXPERIMENTAL MODEL AND SUBJECT DETAILS

Mice

Male and female mice of Dectin-1$^{(-/-)}$ KO (B6.129S6-*Clec7a*^{tm1Gdb}/J) and Dectin-1 wild-type (WT; C57BL/6J) littermates were maintained and bred under specific pathogen-free conditions at the animal facility of the German Cancer Research Center, Heidelberg. All animal studies were approved by the veterinary authorities (Regierungspräsidium Karlsruhe) of Baden-Württemberg (DKFZ346 and G291-14). NOX-2 KO mice were generated by M. C. Dinauer and are available from JAX (https://www.jax.org/strain/002365; Pollock et al., 1995). Littermates of gp91$^{phox\ (Y/X-)}$ KO (B6.129S-Cybb$^{tm1Din/J}$) and gp91$^{phox\ (Y/X+)}$ WT male mice were bred using heterozygous gp91$^{phox\ (X+/X-)}$ female and hemizygous gp91$^{phox\ (Y/X-)}$ KO male mice. The mice were bred under standard conditions at the animal facility of the *Centre Médical Universitaire* of the Faculty of Medicine, University of Geneva. No obvious problems regarding infections were observed in these mice.

Cell Lines

The human T cell line Jurkat E6.1 (Schneider et al., 1977) was cultured in RPMI 1640 (Sigma-Aldrich) supplemented with 10% FCS. Murine RMA cells stably expressing OVA in the cytoplasm (Tiwari et al., 2007) were cultured using RPMI 1640 supplemented with 10% FCS, 50 μM 2-Mercaptoethanol (Sigma-Aldrich) and 100 μg/ml Geneticin sulfate (G418; GERBU Biotechnik). Human Mono Mac 6 (MM6; Ziegler-Heitbrock et al., 1988) cells were cultured in RPMI 1640, 10% FCS and 1% OPI-supplement (SIGMA-Aldrich). *Drosophila melanogaster* S2 cells (S2-cells) stably expressing murine Annexin A1 (mAnxA1) and membrane-anchored OVA (S2-mAnxA1/OVA cells) were generated previously (Linke et al., 2015). S2-mAnxA1/OVA cells were cultured in Schneider's insect medium (Sigma-Aldrich) supplemented with 10% FCS and Hygromycin B (PAA). The human hDectin-1b-expressing HEK293 NF-κB reporter cell-system was obtained from Invivogen and cultured according to the manufacturer's instructions.

METHOD DETAILS

Preparation of Bone-Marrow–Derived Dendritic Cells

Bone marrow (BM)-derived dendritic cells (DCs, BMDCs) were prepared from male or female mice between 6 and 14 weeks (wks) of age, as described before (Linke et al., 2015). In brief: BM cells were flushed from *tibias* and *femurs*, and red blood cells were lysed by brief exposure to 0.168 M NH_4Cl and further washed twice with RPMI 1640 (Sigma-Aldrich) supplemented with 10% FCS (Sigma-Aldrich). For differentiation of BM precursors to BMDCs using recombinant murine GM-CSF (Immunotools), cells were seeded at a density of 0.5x10^6 cells/ml in BMDC medium (RPMI 1640 with 10% FCS and 20 ng/ml GM-CSF) in a 24-well plate. After 2 d, the medium was carefully replaced by fresh BMDC medium (37°C). After 5 d, half of the medium was removed and replaced by fresh BMDCs medium (37°C). Experiments were conducted on d 6 of differentiation. The differentiation of BM precursors to BMDCs was monitored by flow cytometric analysis using monoclonal antibodies (mAbs) against CD11b, CD11c, CD80, CD86, PD-L1, DEC-205, MHC class II and Dectin-1 (listed in Key Resources; data not shown).

Flow Cytometry

All staining procedures were performed in PBS/10%FCS/10% mouse or rat serum. Abs and reagents used for FACS were purchased from BioLegend (anti-mCD86-APC-Cy7, anti-mCD11c-APC, anti-mMHC class II-PerCP-Cy5.5, anti-mF4/80-APC-Cy7, anti-mCD80-FITC, anti-mPD-L1–PE, anti-mDEC-205-PE-Cy7), eBioscience (anti-p-SYK (Tyr348)PE, anti-hDectin-1-PE), Caltag (anti-mCD11b-PE), BD Biosciences (anti-mCD80-PE), LIFE Technologies (anti-hSYK-APC) and Abcam (anti-mDectin-1-FITC). Appropriate isotype controls were purchased from Biolegend or eBioscience. Phosphatidylserine exposure and cellular membrane integrity were analyzed by staining with annexin A5 (AnxA5)-FITC (Immunotools) or AnxA5-APC (Immunotools) and 7-aminoactinomycin D (7-AAD; Sigma-Aldrich), respectively (data not shown). Stained cells were analyzed on a FACS Canto II (BD Biosciences) with FlowJo software (BD Biosciences).

Antibodies, ELISA, and Reagents

Anti-human (h) annexin A1 (AnxA1) (DAC5) and Anti-mouse AnxA1 (mAx550) Abs were generated in our laboratory (Weyd et al. 2013). Intracellular p/total-SYK staining's were performed with or without the phosphatase inhibitor sodium vanadate (Sigma-Aldrich; 1mM) as indicated, and by permeabilization with Methanol (100%) for 10min by 4°C. Cytokine concentrations in supernatants were

determined by ELISA for mIL-12p40 (PeproTech), m/hIL-6, hTNFα (both BD Biosciences), according to the manufacturers' instructions. Western Blot (WB) detection of human p-SYK was performed using following antibodies against: p-SYK (Tyr525/526; Cell Signaling Technology), p-SYK (Tyr348; Abcam), p-SYK (Tyr352; Cell Signaling Technology) and total SYK (Cell Signaling Technology). Auto-Abs against double-stranded (ds) DNA were determined by ELISA developed in our laboratory as follows: 10μg/ml dsDNA (from calf thymus, SIGMA) was captured in coating buffer (0.2 M sodium phosphate buffer, pH 6.5) overnight on 96-well plates (round-button, LIFE Technologies) at 4°C. After blocking for 1 h in 1% Casein (in PBS) on RT, mouse blood plasma samples (1/50 in PBS/10% FCS) were added for 2h. The binding of anti-dsDNA Abs was detected by horseradish peroxidase-conjugated Ig (isotype)-specific anti-m Abs (goat anti-mIgM, μ chain specific, Jackson ImmunoResearch Labs; goat anti-mIgG1, SouthernBiotech; goat anti-mIgG2b, SouthernBiotech; goat anti-mIgG3, SouthernBiotech; goat anti-mIgG2c, Abcam; anti-mIg, Thermo Fisher Scientific) using the substrate o-Phenylenediamine (Thermo Fisher Scientific) and the absorbance of 490nm was measured. Laminarin, dispersible whole glucan particle (dWGP), depleted zymosan (DZ) and β-glucan peptide (BGP) were purchased from Invivogen. DZ (1 mg/ml) was filtered using membranes with different pore sizes (0.2 μm; 0.45 μm; 35 μm) to obtain the soluble fraction of β-glucans. The concentration of filtered DZ was not determinable but the majority of DZ is present as large particles. Bovine extracted catalase was purchased from Carl Roth. 6-Hydroxy-2,5,7,8-tetramethylchroman-2-carboxylic acid (Trolox) was obtained from Th. Geyer. SYK inhibition experiments were performed using SYK-inhibitor-2 (200nM). Specific NADPH-oxidase 2 (NOX-2) inhibition experiments were performed using the peptide inhibitor *gp91 ds-TAT* aside with appropriate control *scrambled gp91 ds-TAT* (Anaspec), and the small molecule inhibitor GSK2795039 diluted in DMSO (MedChem Express). Splenic DCs and macrophages were isolated using collagenase Typ IV (Biochrome) and DNase I (Roche).

Transfections and CRISPR/Cas9-Mediated Genome-Editing

The plasmid for hDectin-1b (Invivogen) was transfected using AMAXA Cell Line Nucleofector Kit V (Lonza). To generate stably transfected MM6, cells were selected using Blasticidin S Hydrochloride (Thermo Fisher Scientific) for 21 to 28 d or, if necessary, were separated via FACS using a fluorescently labeled anti-Dectin-1 Ab after 3 to 14 d of Blasticidin selection. Dectin-1-deficient MM6 cells were generated using CRISPR/Cas9 genome-editing technology as described previously (Ran et al., 2013). In brief: Dectin-1-specific guide (g)RNAs (gRNA1: 5′-AACTTGTTTCACGCTATATC; gRNA2: 5′-AAGATGTGCTTCGAGATGTG) targeting Exon 1 were cloned into the pSpCas9(BB)-2A-GFP Vector (Addgene) that encodes Cas9 linked with a 2A spacer to GFP. Dectin-1-specific Cas9-GFP vectors were transfected into MM6 cells using AMAXA-Nucleofection technology. After 24 to 48 h, GFP-positive cells were isolated by FACS. After incubation for 5-7 d, cells were clonally separated in 96-well plates by limiting dilution (0.1 cells / well) using RPMI 1640 with 10% FCS, 1% OPI-supplement and 10 U/ml penicillin/streptomycin (Sigma-Aldrich). After 2-4 wks, DNA from expanded clones was isolated and the Dectin-1 targeted locus was amplified by PCR. After PCR purification the Dectin-1 target locus was analyzed by Sanger sequencing (listed in Key Resources Table). Homozygous Dectin-1 nonsense mutations were confirmed by Sanger-sequencing. Loss of Dectin-1 expression was verified by flow cytometry using Dectin-1 specific mAb and by qPCR. MM6 Dectin-1 KO clones 1 and 2 were generated in two independent experiments.

Generation and Purification of Recombinant Proteins

Plasmids for murine (m)AnxA1ΔN, mAnxA1, mAnxA5 and human (h)AnxA1ΔN were generated and purified as described previously (Linke et al., 2015). For transformation, 100 μL of competent *E. coli* bacteria were incubated on ice for 30 min with 10 ng plasmid DNA. After a 30 s heat pulse at 42°C the suspension was incubated on ice for 2 min and subsequently regenerated for 1 h at 37°C in 450 μl SOC-medium (New England Biolabs). Finally, the bacteria were streaked on LB-agar plates with suitable selection medium. Bacterial colonies grew overnight at 37°C. Recombinant annexins were expressed and purified in our laboratory as previously described (Linke et al., 2015) using the *E. coli* strain Rosetta (DE3; Novagen). In brief: Expression for 20 h at 18°C after induction with 1 mM Isopropyl β- d-1-thiogalactopyranoside (IPTG; Carl Roth) yielded highest solubility of recombinant annexins. To increase protein production, bacterial cultivation was conducted in baffled conical flasks. Bacteria were lysed in the presence of Benzonase (Roche) through successive freeze and thaw cycles in liquid nitrogen and a 38°C water bath, respectively. Soluble annexins were purified after bacterial lysis via its C-terminal Protein A-tag that binds to immunoglobulin G (IgG)-coated beads. Reduction of lipopolysaccharides (LPS) contamination was achieved by washing with TBS buffer containing 0.1% Triton X-114 (SIGMA-Aldrich). PreScission protease (GE Healthcare) was used to cleave recombinant annexin from its purification tag. Glutathione beads (GE Healthcare) then served to remove the glutathione-S-transferase (GST)-tagged protease. Finally, the recombinant protein was cleared from LPS by ion-exchange purification. The mAnxA1 core domain (mAnxA1ΔN) was also expressed in eukaryotic *Spodoptera frugiperda* Sf9 insect cells using baculovirus. The virus DNA was generated using the Bac-to-Bac® Baculovirus Expression System (Invitrogen) in combination with the pFastBac-M30a vector encoding for mAnxA1ΔN. Following lysis of the cells in the presence of Benzonase and complete protease inhibitor (Roche), insoluble debris was removed via centrifugation for 30 min at 40,000 rpm. Soluble GST-tagged mAnxA1ΔN was purified from lysate using a 5 mL Protino GST/4B column (GE Healthcare). After washing, mAnxA1ΔN was cleaved from the column using GST-tagged 3C protease. Finally, mAnxA1ΔN was dialyzed into sodium phosphate based low salt buffer and freed from LPS through anion exchange chromatography. The production and purification of eukaryotic mAnxA1ΔN was performed by the Protein Expression and Purification Core Facility at the European Molecular Biology Laboratory (EMBL), Heidelberg

(Stolt-Bergner et al., 2018). LPS content in all annexin preparations was determined to be below 0.001 EU/μg using the Limulus amoebocyte lysate assay (Lonza) according to the manufacturer's instructions. If not stated otherwise, procaryotically produced Anx was used.

Preparation of Apoptotic Cells (ACs)

For induction of apoptosis, $1x10^6$ cells/ml in a total volume of 2.5 ml/well (in 6-well cell culture-treated plates) were irradiated with 75 mJ/cm^2 (Jurkat T cells), 500 mJ/cm^2 (RMA-OVA cells) or 1000 mJ/cm^2 (S2-mAnxA1/OVA UV-C in a Stratalinker 1800 (Stratagene/Agilent Technologies) and used after 2–2.5 h (Jurkat T cells and RMA-OVA cells) or 16-20h (S2-mAnxA1/OVA) of incubation in RPMI/10% FCS at 37°C as previously described (Linke et al., 2015). During apoptosis, cytosolic annexins are externalized to the cell surface of apoptotic cells. About 2 h (Jurkat T cells and RMA-OVA cells) or about 16 h (S2-mAnxA1/OVA) after UV-irradiation membrane (PS)-bound AnxA1, AnxA5 and AnxA13 can be detected such as by flow cytometry using fluorescently labeled anti-Anx mAbs (see Key Resources Table; Linke et al., 2015; Weyd et al., 2013; and data not shown).

In Vitro Suppression-Assay with ACs or Recombinant Proteins

A total of $1x10^5$ BMDCs or MM6 cells were incubated with recombinant protein (100-1000 nM), DZ, apoptotic Jurkat T cells ($0.1\text{-}4x10^5$ cells) or apoptotic RMA cells ($4x10^5$ cells) in the presence of the LPS neutralizing agent Polymyxin B (PmxB; 50μg/ml final concentration) for 4-8 h. Cells were subsequently stimulated with 10-60 nM CpG 1668 (Invivogen; BMDCs) or 0,5-1 μg/ml R848 (Invivogen; MM6 cells). Cytokine concentrations in the supernatants were analyzed by ELISA 16-24 h after TLR stimulation. CD80 surface expression was measured 2-3 d after TLR stimulation. If not stated otherwise: The suppression of cytokine secretion was normalized to CpG-stimulation minus background (100 - ((treated - untreated) / (CpG only - untreated)) *100).

RNA Isolation and Quantitative RT-PCR

RNA was isolated from cells using the RNeasy Maxi Kit (QIAGEN) or RNAqueous-Micro Kit (Ambion), according to the manufacturers' instructions. Reverse transcribed RNA was quantified by detection of SYBR Green (Sigma-Aldrich) incorporation using the ABI Prism 7500 sequence detector system (Applied Biosystems). Expression levels were normalized to mHMBS or hHPRT1.

Detection of Reactive Oxygen Species (ROSs)

Intracellular amounts of ROSs in BMDCs, MM6 and Jurkat T cells were determined using ROS sensitive H_2DCFDA (Sigma-Aldrich). For this, $1x10^5$ cells/well were seeded in RPMI/10% FCS, supplemented with 50 μg/ml of PmxB (Sigma-Aldrich) to exclude LPS-mediated effects. Treatments such as PMA or annexins were added 1 h later and cells were incubated for 0 to 2.5 h at 37°C. Following treatment, 5 μM of H_2DCFDA was added for 0.5 h. The reaction was stopped by addition of 25 μM of the hydroxyl radical scavenger Trolox or 20mM of the antioxidant N-acetyl-L-cysteine (NAC; Sigma-Aldrich) for 10-15 min. Afterward, cells were kept on ice in the dark and washed with ice cold RPMI/10% FCS supplemented with 100 μM Trolox or 20 mM NAC to slow down cell metabolism. ROS production was quantified by flow cytometry within the FITC-channel (Ex: 488nm/ Em: 519nm). The indicated mean fluorescence intensity (MFI)-increase was normalized to untreated (or control treated) cells ((MFI treated – MFI untreated) / MFI untreated * 100). Extracellular H_2O_2-release was determined 2 h after treatment using the *Amplex Red Hydrogen Peroxide/Peroxidase Assay Kit* (LIFE Technologies) according to the manufacturer's instructions.

Annexin-Coated Vesicle Production

Lipid vesicles for initial binding experiments (Figure S3B) were generated by sonication. Phosphatidylcholine (PC, 1,2-dioleoyl-sn-glycero-3-phosphocholine) and phosphatidylserine (PS, 1,2-dioleoyl-sn-glycero-3-phospho-L-serine) (both purchased from Avanti Lipids Polar) were mixed in a 5:1 ratio (PC:PS), supplemented with 50 μg/ml endotoxin-free OVA (invivogen) and suspended in Chloroform (≥99.5%, Sigma-Aldrich). After evaporation using a Concentrator 5301 with vacuum degassing equipment (Eppendorf), the dry lipid/OVA-pellet was resuspended in DPBS (Ca^{2+} and Mg^{2+} included; DPBS^{2+}; Sigma-Aldrich) and sonicated with a *SONOPULS HD 2070* device (Bandelin, at Cycle 5, 30% power) for 1 min. Lipid vesicles were centrifuged for 30 min by 18,000xg at 4°C. After removing the supernatant, lipid vesicles were resuspended in DPBS. For the preparation of annexin-coated vesicles, an aliquot of lipid vesicles was diluted 1:5 in DPBS^{2+} supplemented with hAnxA1ΔN (50 μg/ml) and incubated over night at 4°C on a roll shaker. Unbound annexin was removed by centrifugation for 30 min at 18,000xg and 4°C and following resuspension with DPBS^{2+}. The degree of annexin-loading was analyzed using anti-hAnx-FITC mAb generated in our laboratory (Weyd et al., 2013). Size-defined PS-containing vesicles (400 nm) used for competition and functional experiments were generated by extrusion based on a protocol obtained from W. Nickel and colleagues (Temmerman and Nickel, 2009). 18:1 (9-*Cis*) PC (DOPC), 18:1 PS (DOPS) and Cy5 labeled phosphatidylethanolamine (Cy5-PE) (all from Avanti Polar Lipids) suspended in chloroform (Sigma-Aldrich) were mixed with a molar ratio of 79% DOPC, 20% DOPS and 1% Cy5-PE in a 10 mL glass round-bottom flask. Lipids were handled in glassware to prevent chloroform-mediated plastic contaminations. The lipid mixture was dried under vacuum for approximately 4 h. The remaining lipid layer was dissolved in 50°C pre-warmed PBS containing 10% sucrose (Merck) vortexing by short-time at a constant temperature of 50°C. Next, the lipid solution was frozen in liquid nitrogen and subsequently thawed ten times at 50°C in order to exclude the formation of multi-lamellar liposomes. An extruder with a 400 nm pore size membrane was used and the lipid mixture was pushed through the membrane 21 times to achieve homogenization of the vesicle size. The synthesized lipid-vesicles were washed twice

with DPBS and centrifuged at 18,000xg for 20 min at 4°C. For the preparation of annexin-coated vesicles, 200μl of the lipid-vesicle stock mixture diluted 1:5 in $DPBS^{2+}$ and supplemented with hAnxA1ΔN (50 μg/ml) was incubated over night at 4°C on a roll shaker. Residual annexin was removed by centrifugation at 18,000xg for 90 min at 4°C and the vesicles were resuspended in 200 μl $DPBS^{2+}$. The degree of annexin-loading was analyzed using anti-hAnx-FITC mAb generated in our laboratory (Weyd et al., 2013). Using BD Trucount Tubes (BD Biosciences), we determined a vesicle concentration of about 30,000 vesicles/μl with approximately 2.6 pg of coated hAnxA1ΔN/vesicle calculated semiquantitatively via WB (data not shown).

Attana Cell 200 Quartz Crystal Microbalance (QCM) Analysis

Attana Cell 200 is a dual channel, continuous-flow system for automated analysis of molecular interactions based on quartz crystal microbalance (QCM) technology (Peiris et al., 2017; Salanti et al., 2015). To monitor binding interactions, one of the interacting molecules is immobilized on the sensor surface and the sample containing the other molecule of interest is injected over the immobilized molecule. The signal output is given in frequency (Hz) and is directly related to changes in mass on the sensor surface. The negative changes of resonance frequency are depicted. Dectin-1 expressing and Decitn-1 KO MM6 cells were immobilized on Attana sensor surfaces using a capturing approach. Cell suspensions were centrifuged, and the cell pellets were rinsed briefly three times with PBS (Thermo Fisher Scientific) to remove cell media. Cell pellets were then resuspended in PBS to a final density of $2x10^6$ cells/ml. Immobilization of the capturing molecule concanavalin A (ConA) on LNB carboxyl surfaces (3623-3001) was performed using Attana amine coupling kit (3501-3001). 150 Hz of ConA was stably immobilized on the surfaces. Cells were captured on surfaces by incubating 10^5 cells in PBS for 30 min at RT. Following incubation, the cells were rinsed three times with 0.7 mL PBS at RT and stabilized in fresh 4% (v/v) methanol-free formaldehyde (Thermo Fisher Scientific) for 15 min at 4°C. Cell coverage was determined by staining cells with 3 μM DAPI (Merck) and visualized under fluorescent microscope (data not shown). Sensor surfaces were inserted in the biosensor or stored under humidity at 4°C in the dark until use. Interaction of the analytes with cell surfaces was assessed using Attana Cell 200 biosensor. Initial binding experiments were performed at a flow rate of 20 μl/min at 22°C. All experiments were performed under continuous flow of PBS (with $CaCl_2$ + 0.1% FCS). A blank injection of PBS (with $CaCl_2$ + 0.1% FCS) was performed before each analyte injection. The blank injection was subtracted from the subsequent analyte injection to correct for baseline drift. One analyte at a time was injected for 105 s over the cell surfaces. For kinetic experiments, four two-fold dilutions of each analyte were injected over cell surfaces. Surface regeneration was carried out using a 30 s injection of glycine 10 mM (pH 2.2). Repeated injections of the same analyte concentration resulted in identical binding curves, indicating that regeneration did not alter the binding capacity of the surface. For competitive binding analysis the cells were coated on the sensor surface as described above. Single cycle kinetics and competition assays were performed at a flow rate of 10 μl/min at 22°C with a continuous flow of PBS. Single cycle kinetic experiments were performed to determine the saturation levels (B_{max} values) of each analyte for the given surface. hAnxA1ΔN-coated vesicles were injected into the flow cell over Dectin-1-expressing MM6 cells until saturation (B_{max}). A mixture of hAnxA1ΔN-coated vesicles and DZ (1:1) was further injected over the saturated surface. Experiments were also performed in the reverse order, i.e., injecting DZ before the mixture. The frequency change in the sensor surface resonance (ΔF) during the binding experiments was recorded using the Attester software (Attana AB) and the data were analyzed using the Evaluation (Attana AB) and TraceDrawer software (Ridgeview Instruments) using 1:1 or 1:2 binding models to calculate the kinetic parameters including the rate constants (k_a, k_d), dissociation equilibrium constant (K_D) and the maximum binding capacity (B_{max}). Simulation curves were generated using Evaluation (Attana AB) software.

Production of the CLR-Fc Fusion Protein Library and ELISA Binding Experiments

The library of CLR-Fc fusion proteins was prepared as described previously (Maglinao et al., 2014). Briefly, murine splenic RNA was reverse transcribed into cDNA using Reverse Transcriptase (New England Biolabs). The cDNA encoding the extracellular part of each CLR was amplified by polymerase chain reaction (PCR) and was then ligated into the pFuse-hIgG1-Fc expression vector (Invivogen). The CLR-Fc vector constructs were either stably transfected into CHO cells or transiently transfected using the FreeStyle Max CHO-S Expression System (Thermo Fisher Scientific). Purification of the CLR-Fc fusion proteins from the cell supernatant was performed using HiTrap Protein G HP columns (GE Healthcare). The purity of each CLR-Fc fusion protein was confirmed by sodium dodecyl sulfate polyacrylamide gel electrophoresis (SDS-PAGE) and subsequent Coomassie staining, Western Blot using anti-human IgG-HRP antibody (Dianova) as well as mass spectrometry. mAnxA1 (0,5 μg/well) and mAnxA5 (0,5 μg/well) were coated on 96-well high binding plates (Greiner) overnight. After blocking with 1% BSA in PBS, 20 μg/mL of each CLR-Fc fusion protein was incubated in lectin binding buffer (50 mM HEPES, 5 mM $MgCl_2$, 5 mM $CaCl_2$, pH 7.4) at RT for 2 h. The binding of CLR-Fc fusion proteins was detected by an alkaline phosphatase-conjugated goat anti-hFc antibody (Dianova). Development was performed with p-nitrophenyl phosphate (Thermo Scientific). For binding experiments in Figure 1B recombinant mAnxA1 or mAnxA5 (both 20 μg/ml) were coated in coating buffer (BD Biosciences; supplemented with 5mM $CaCl_2$) on 96-well plates (Greiner) overnight. After blocking in PBS/2%BSA/5mM $CaCl_2$ solution for 2h, mDectin-1 Fc fusion protein (solved in PBS/0.2%BSA/5mM $CaCl_2$) was incubated at RT for 2 h. The binding of mDectin-1 Fc to indicated annexins was detected by horseradish peroxidase-conjugated anti-mIg (Thermo Fisher Scientific) using the substrate o-Phenylenediamine (Thermo Fisher Scientific). The absorbance by 490 nm was measured.

Surface Plasmon Resonance (SPR) Analysis

Binding analyses were carried out on a Biacore T100 instrument (GE Healthcare). CM5 sensor chips were functionalized with about 10,000 RUs of AnxA1 using the Amine Coupling Kit (GE Healthcare) according to the manufacturer's recommendations. Kinetic measurements were performed with the Biacore T100 Control software using the 'Kinetics' function. HEPES (10 mM) containing $CaCl_2$ (1 mM), $MgCl_2$ (1 mM), 0.005% Tween pH 7,4 was used as running buffer and all measurements were performed at 25 °C and a flow rate of 30 μl min^{-1}. About 500 RUs of fusion proteins were captured and the indicated concentrations were passed through using the standard parameters for association and dissociation times. Flow cells were regenerated with 10 mM glycine-HCl pH 1.7 for 30 s. Kinetic evaluation of binding responses was performed with the Biacore T100 Evaluation software.

In Vivo Experiments

A total of $2x10^6$ apoptotic S2-mAnxA1/OVA cells were injected (*s.c.*) into the right flank on day 0 and 7. Mice were sacrificed on day 14 and draining inguinal lymph nodes (dLN) were analyzed for OVA-specific $CD8^+$ T cells using SIINFEKL-Dextramers (Immudex). Serum was taken 1 day before the first injection, three days after the first injection and on day 14. The serum level of soluble urokinase receptor (uPAR) was determined by ELISA (Hölzel Diagnostika).

QUANTIFICATION AND STATISTICAL ANALYSIS

All data are shown as mean values ± standard deviation (s.d.) unless indicated otherwise. Sample numbers of data obtained from animal experiments refer to the number of individual mice, as specified in the figure legends. Statistical analysis of data was performed by unpaired or paired student's t test as well as by Mann Whitney test, as indicated in the figure legends. If not otherwise indicated, the significance of the difference compared with WT cells or control treated cells is depicted. The ρ values < 0.05 were considered statistically significant using the GraphPad Prism software, as indicated in the figure legends.

DATA AND CODE AVAILABILITY

This study did not generate new, unique, data or code.